ECOSTRESS estimates gross primary production with fine spatial resolution for different times of day from the International Space Station

Xing Li[a], Jingfeng Xiao[a*], Joshua B. Fisher[b], Dennis D. Baldocchi[c]

[a] Earth Systems Research Center, Institute for the Study of Earth, Oceans, and Space, University of New Hampshire, Durham, NH 03824, USA

[b] Jet Propulsion Laboratory, California Institute of Technology, 4800 Oak Grove Dr., Pasadena, CA 91109, USA

[c] Department of Environmental Science, Policy, and Management, 137 Mulford Hall, University of California at Berkeley, Berkeley, CA 94720, USA

*Correspondence to: j.xiao@unh.edu

Abstract: Accurate estimation of gross primary production (GPP), the amount of carbon absorbed by plants via photosynthesis, is of great importance for understanding ecosystem functions, carbon cycling, and climate-carbon feedbacks. Remote sensing has been widely used to quantify GPP at regional to global scales. However, polar-orbiting satellites (e.g., Landsat, Sentinel, Terra, Aqua, OCO-2) lack the capability to examine the diurnal cycles of GPP because they observe the Earth's surface at the same time of day. The Ecosystem Spaceborne Thermal Radiometer Experiment on Space Station (ECOSTRESS), launched on June 2018, observes the land surface temperature (LST) at different times of day with high spatial resolution (70 m × 70 m) from the International Space Station (ISS). Here, we made use of ECOSTRESS data to predict instantaneous GPP with high spatial resolution for different times of day using a data-driven approach based on machine learning. The predictive GPP model used instantaneous ECOSTRESS LST observations along with the daily enhanced vegetation index (EVI) from the Moderate Resolution Imaging Spectroradiometer (MODIS), land cover type from the National Land Cover Database (NCLD), and instantaneous meteorological data from the ERA5 reanalysis dataset. Our model estimated instantaneous GPP across 56 flux tower sites fairly well (R^2 = 0.88, Root Mean Squared Error (RMSE) = 2.42 μmol CO_2 m^{-2} s^{-1}). The instantaneous GPP estimates driven by ECOSTRESS LST captured the diurnal variations of tower GPP for different biomes. We then produced multiple high resolution ECOSTRESS GPP maps for the central and northern California. We found distinct changes in GPP at different times of day (e.g., higher in late morning, peak around noon, approaching zero at dusk), and clear differences in productivity across landscapes (e.g., savannas, croplands, grasslands, and forests) for different times of day. ECOSTRSS GPP also captured the seasonal variations in the diurnal cycling of photosynthesis. This study demonstrates the feasibility of using ECOSTRESS data for producing instantaneous GPP (i.e., GPP for the acquisition time of

the ECOSTRESS data) for different times of day. The ECOSTRESS GPP can shed light on how plant photosynthesis and water use vary over the course of the diurnal cycle and inform agricultural management and future improvement of terrestrial biosphere/land surface models.

Keywords: Gross primary productivity; Land surface temperature; Diurnal cycle; Photosynthesis; Water use efficiency; Carbon cycle; Geostationary satellite; MODIS; Stomatal conductance; Earth system model

1. Introduction

Photosynthesis, the underlying process of terrestrial vegetation, constitutes the largest flux of the global carbon cycle. Quantifying the spatial and temporal dynamics of photosynthesis at the ecosystem scale (i.e., gross primary production, GPP) can provide important information on the magnitude and variability of terrestrial carbon budget and carbon-climate feedbacks (Beer et al. 2010; Xiao et al. 2014). Previous studies showed the feasibility of estimating GPP at different temporal scales (e.g., daily, monthly, annual) (Zhao et al. 2005; Xiao et al., 2010; Gilabert et al. 2015). The seasonal and interannual variations of GPP are found to be driven by climate variability, plant phenology, and changes in physiological capacity due to nutrient status and soil moisture deficits (Li and Xiao 2020; Mäkelä et al. 2006; Xia et al. 2015; Xu and Baldocchi 2004). Diurnal variations (or diel variations) of GPP are mainly driven by environmental (e.g., solar radiation, air temperature, soil moisture, vapor pressure deficit or VPD) and physiological (e.g., stomatal conductance) factors (Damm et al. 2010; Franco and Lüttge 2002; Paul-Limoges et al. 2018). Diagnosing the diurnal variations of GPP can provide insights into direct interactions between photosynthesis and these controlling factors, which otherwise would be obscured by aggregating the instantaneous variables to daily or seasonal scales.

The eddy covariance (EC) technique provides temporally (half-hourly or hourly) continuous measurements of ecosystem-level GPP over the course of the diurnal cycle (Baldocchi et al. 2001). However, these EC flux towers provide only spatially sparse GPP estimates due to their sparse distributions across the globe (Xiao et al. 2010). Satellite observations make up for the limitation in spatial representation and global coverage of the EC technique and can lead to spatially continuous GPP estimates from regional to global scales based on different approaches (Xiao et al. 2019), including light use efficiency models (Running et al. 2004; Zhao et al. 2005; Stocker et

al. 2020), terrestrial biosphere models (Liu et al. 1997; Ryu et al. 2011), and data-driven approaches (Beer et al. 2010; Xiao et al. 2010). During the past decades, GPP has been successfully estimated from polar-orbiting satellites, such as Landsat (30 m, 16-day) (Gitelson et al. 2012; Robinson et al. 2018), Terra/Aqua (500 m, 8-day) (Running et al. 2004; Zhao et al. 2005; Xiao et al. 2010), Sentinel-2 (up to 10 m, 5 day) (Lin et al. 2019b; Wolanin et al. 2019), and OCO-2 (Li and Xiao 2019a). However, polar-orbiting satellites lack the capability to examine the diurnal cycle of GPP because they observe the Earth's surface at the same time of day for every revisit. Fortunately, the recent launch of the Ecosystem Spaceborne Thermal Radiometer Experiment on Space Station (ECOSTRESS) provides an unprecedented yet unexplored opportunity for examining the variations of plant carbon uptake over the course of a day on large scales.

ECOSTRESS, managed by National Aeronautics and Space Administration (NASA)'s Jet Propulsion Laboratory (JPL), was launched to the International Space Station (ISS) on 29 June 2018. ECOSTRESS uses a multispectral thermal infrared radiometer to measure radiance in five bands from 8 to 12.5 μm and an additional band at 1.6 μm for geolocation and cloud detection (http://ecostress.jpl.nasa.gov). On board the ISS with an inclined, precessing orbit, ECOSTRESS can measure the Earth's surface at different times of day from 53.6° N to 53.6° S, which is promising to capture diurnal biological processes that are unexploited by traditional polar orbiting, sun-synchronous platforms with a fixed equator crossing time (e.g., Landsat, Sentinel, Terra, Aqua, OCO-2). ECOSTRESS has a high spatial resolution of 38 m × 69 m (at nadir) and frequent revisit time of 1–5 days depending on the latitude (Fisher et al. 2015, 2020). The combination of diurnal sampling capability and fine spatial and temporal resolutions endows ECOSTRESS with a great potential for sampling the diurnal variation of terrestrial ecosystems, even for individual farmers' fields. ECOSTRESS can provide key insights into plant–water dynamics, ecosystem–climate

interactions, and agricultural management. It also has potential to answer how do snapshots of remote sensing scale with daily integrals across different biomes and latitudinal zones (Sims et al. 2005; Ryu et al. 2012).

The ECOSTRESS mission measures the temperature of plants from space, and provides both land surface temperature (LST) and emissivity (Level-2 products) at a spatial resolution of ~70 m × 70 m (Hook et al. 2019; Hulley et al. 2019). LST is one of the important parameters for studying processes at the land-atmosphere interface which measures Earth's surface temperature rather than air temperature. For plants, many physiological or biological activities (e.g., transpiration, photosynthesis) of canopy (or leaves) are closely associated with the variations in LST, and therefore LST is widely used as a key variable for estimating evapotranspiration (ET) (Su et al. 2002; Nagler et al. 2005; Jin et al. 2011) and GPP (Sims et al. 2008; Xiao et al. 2010; Schubert et al. 2010). Currently, no other satellite sensors have such sufficient spatio-temporal resolution to reliably monitoring LST at the local to global scale over the diurnal cycle. For example, the Moderate Resolution Imaging Spectroradiometer (MODIS) on board the Terra and Aqua satellites together provides global coverage of LST only at two times during the daytime and two at night (Fig. 1: 10:30 and 22:30 for Terra and 13:30 and 1:30 for Aqua, local solar time) although with moderate spatial resolution (1 km). Geostationary satellites such as the Geostationary Operational Environmental Satellite (GOES)-R series can capture the diurnal variations of LST (Fig. 1) but with much coarser resolution (2.5-4 km) (Fig. 2b). ECOSTRESS, therefore, provides a unique combination of high spatial and temporal resolution to monitor the temperature of plants over the course of the diurnal cycle (Fisher et al. 2020) (Figs. 1-2).

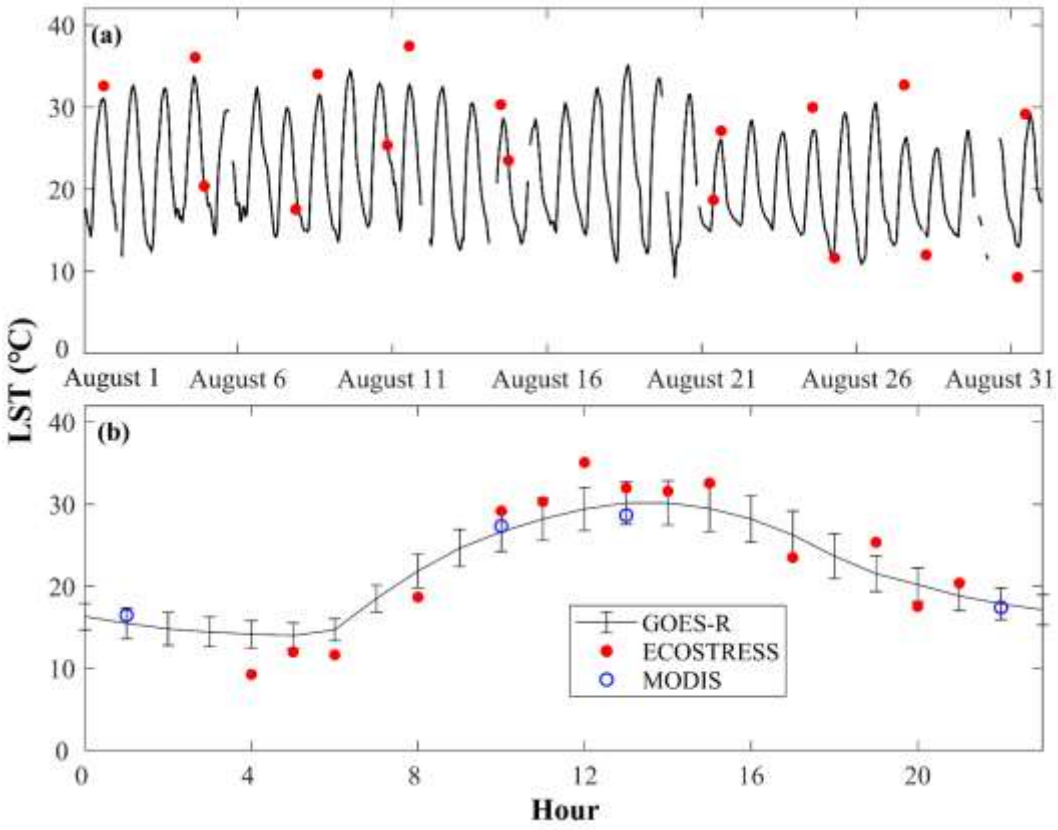

Fig. 1. Diurnal cycle of LST at the Bouldin Island corn site (US-Bi2) during August 2018. (a) shows the LST from GOES-R (GOES-16) and ECOSTRESS from August 1 to August 31, 2018; (b) shows the hourly averaged LST during August: GOES-R provides continuous measurements of hourly LST; MODIS provides LST at only four times of the day; ECOSTRESS measures LST with fine spatial resolution (70 m × 70 m) at different times throughout the day, and therefore can monitor plants over the course of the diurnal cycle with finer spatial resolution.

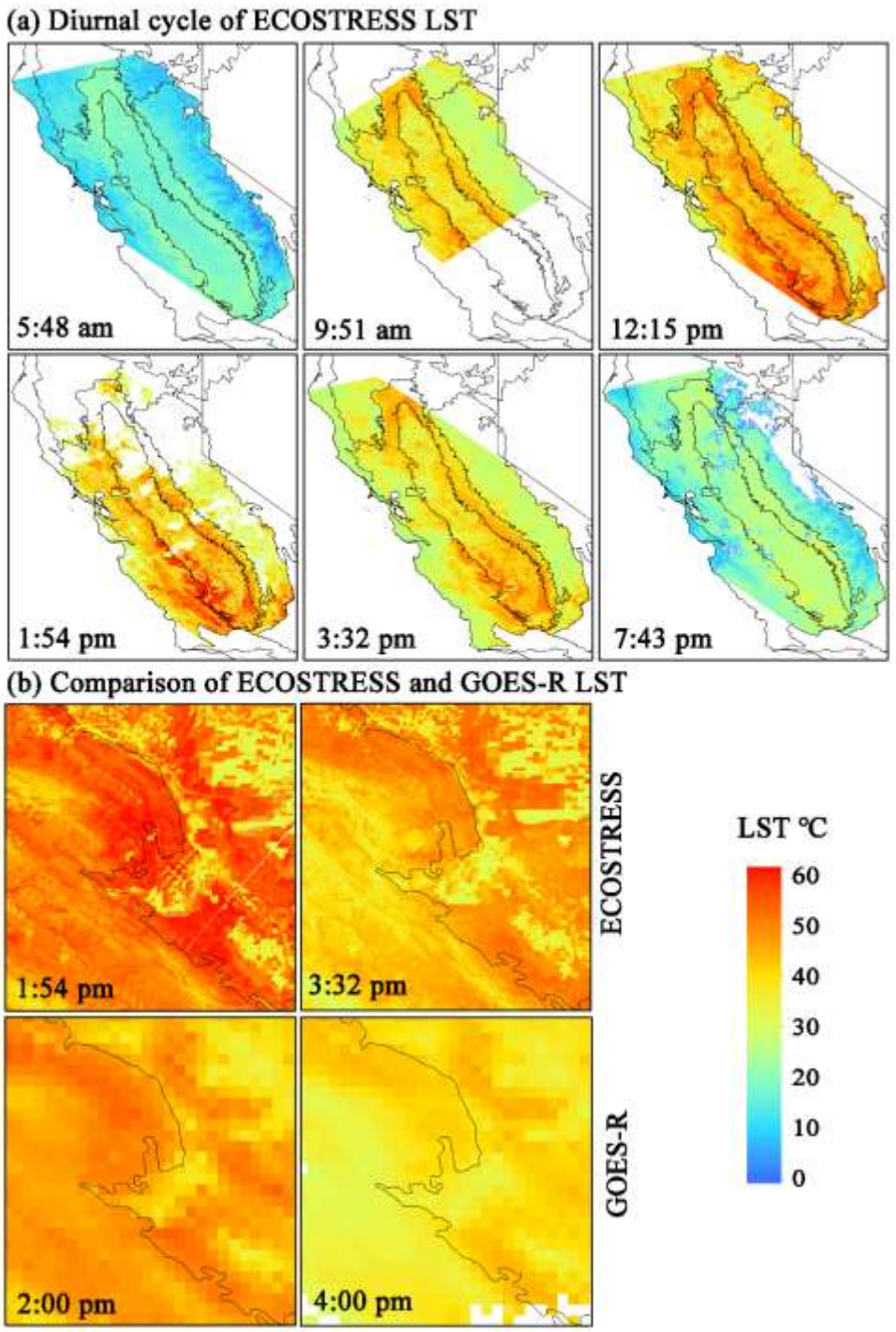

121

122 **Fig. 2.** Diurnal cycle of ECOSTRESS LST across California (a) and comparison of ECOSTRESS and

123 GOES-R LST (b). Both satellites observe LST at different times of day, but ECOSTRESS has much finer

124 spatial resolution (70 m) and much more spatial details than GOES-R (~2 km).

125 Although ECOSTRESS provides a suite of data products (Table S1) such as an instantaneous
126 ET product (a Level-3 product) (Fisher et al. 2008; 2020) and the Level-4 water use efficiency
127 (WUE) product (Fisher & ECOSTRESS algorithm development team, 2018), ECOSTRESS does
128 not offer an instantaneous GPP product. An instantaneous GPP product for different times of day
129 and with fine spatial resolution will be valuable for studying how plants absorb carbon throughout
130 the day in response to the diurnal variations in environmental and physiological factors. In addition,
131 the ECOSTRESS WUE product is based on 500 m, 8-day MODIS GPP (Zhao et al. 2005), not
132 instantaneous GPP, and therefore can only provide WUE information on a daily or 8-day basis and
133 miss the instantaneous variations of WUE over the different times of the day. Having an
134 instantaneous ECOSTRESS GPP product will also allow us to develop instantaneous WUE
135 estimates. Moreover, the synergistic use of such a new instantaneous ECOSTRESS product and
136 the existing instantaneous ET product will allow scientists to identify when plants take up most of
137 carbon or have most water stress over the course of a day, or how water and/or heat stress impacts
138 plant water use and carbon uptake at diurnal timescales across different biomes, towards a better
139 understanding of how plants link Earth's carbon and water cycles.

140 To advance these issues, our presented work here aims to generate instantaneous, high
141 resolution GPP estimates based on instantaneous ECOSTRESS LST data. The 70 m ECOSTRESS
142 LST data along with the EVI from the MODIS, land cover type from the National Land Cover
143 Database (NCLD), and hourly meteorological variables were used for the GPP prediction. We
144 selected California as our study region, to explore whether the ECOSTRESS-based GPP estimates
145 could reasonably capture the diurnal cycle of photosynthesis across biomes. California has high
146 ecological, hydrological, and biological diversity (Fig. 3), and therefore, the estimation of GPP is
147 complicated by the diverse geography, ecosystems, microclimates, and land use and land

148 management across the state (Baldocchi et al. 2019). For example, local ecosystems even have
149 different seasonality due to the complex interactions between diverse ecosystems and
150 environmental and climate drivers (Turner et al. 2020). These characteristics make California an
151 ideal and challenging test bed for us to examine the effectiveness of our method. If ECOSTRESS
152 GPP works well across California, it will increase our confidence in applying our method in other
153 regions of the United States and the globe. Please note that the term 'diurnal cycle' was used to
154 name the full 24 hour period (i.e., the "diel cycle") throughout this paper. To our knowledge, this
155 study is the first effort to predict instantaneous GPP based on ECOSTRESS observations. The
156 availability of instantaneous GPP for different times of day will improve our understanding of how
157 plant photosynthesis and water use vary over the course of the diurnal cycle, and help better
158 manage agricultural irrigation and improve terrestrial biosphere/land surface models.

159 **2. Materials and Methods**

160 *2. 1. Study area*

161 We selected the central and northern California as our study area. This area consists of four
162 ecoregions: the Central California Foothills and Coastal Mountains, Central California Valley,
163 Sierra Nevada, and Coast Range (Fig. 3). The climate of the four ecoregions (defined by Level
164 III Ecoregions map) (Omernik 1987) is mainly characterized by Mediterranean climate with hot
165 dry summers and cool moist winters. The regions with the highest elevation in Sierra Nevada have
166 an alpine climate. The four ecoregions have distinct ecosystem types (Griffith et al. 2016): Coast
167 Range in the west of California is dominated by highly productive evergreen forests; Central
168 California Foothills and Coastal Mountains are primarily composed by woodlands and grasslands,
169 with only patches of pine at high elevations; evergreen forests are the major ecosystems in the

western Sierra Nevada, while juniper woodlands are on the eastern side of Sierra Nevada; Central California Valley is carpeted by vast agricultural regions.

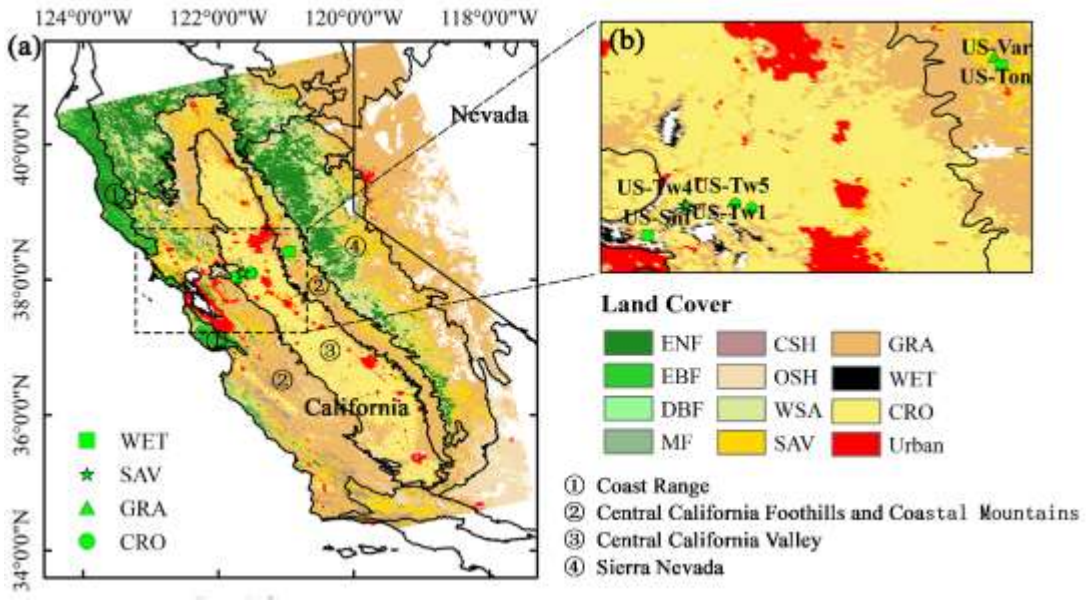

Fig. 3. Our study area consisting of four ecoregions across central and northern California. The base map in (a) is the MODIS land cover map (MCD12Q1, 500m) with the University of Maryland (UMD) land cover classification scheme. The green symbols in the zoomed figure (b) denote the locations of eight EC flux sites used for evaluating the performance of ECOSTRESS-based GPP predictions in Section 3.3. Two crop sites (US-Bi1/Bi2) are overlapped because they are very close to US-Tw1/Tw4/Tw5. The land cover types across the study area include evergreen needleleaf forests (ENF), evergreen broadleaf forests (EBF), deciduous broadleaf forests (DBF), mixed forests (MF), closed shrublands (CSH), open shrublands (OSH), savannas (SAV), grasslands (GRA), croplands (CRO), and wetlands (WET).

2. 2. Data-driven approach, tower GPP, and explanatory data

We used a data-driven method to develop the predictive GPP model, which applied the widely used Cubist (Quinlan 1992), an advanced nonparametric regression tree model, to establish rule-based multivariate linear models between the target variable - GPP and the explanatory variables. Cubist is a traditional vector data mapping algorithm developed in the machine learning domain. The established models can overlap with each other. Specifically, for a set of explanatory variables,

they can match the conditions of one or multiple rules. Cubist may thus generate multiple outputs and take their average as the final GPP prediction. The Cubist model has been successfully applied in our previous studies for predicting spatially and temporally continuous net ecosystem carbon exchange (NEE) (Xiao et al. 2008; Xiao et al. 2011), GPP (Xiao et al. 2010), and SIF (Li and Xiao 2019b). More details on Cubist model were described in these studies. Cubist provides three statistical measures to evaluate the model performance including mean absolute error (MAE), relative error (RE), and the product–moment correlation coefficient (R).

Six explanatory variables were considered for predicting GPP due to their close relationships with GPP and easy data access: LST, shortwave incoming radiation (SW), and VPD for characterizing environmental conditions, daily EVI and annual mean EVI for characterizing vegetation conditions, and land cover type as a categorical variable. The environmental variables showed reasonable regulations on tower GPP (Fig. S1). As air temperature or VPD increased, GPP showed a convex parabolic curve with its peak value occurring around ~25 ℃ and 10 hPa, respectively (Fig. S1a, b). The increase of temperature and VPD would no longer lead to an increase in GPP when environmental conditions start to limit photosynthesis. GPP was also dependent on solar radiation, and high radiation overall corresponded to high productivity. The relationship between LST and tower GPP was similar with that between air temperature and tower GPP, with optimal LST around ~28 ℃.

For training, we were not able to obtain sufficient overpasses of ECOSTRESS LST for robust training due to the recency of the launch. Therefore, we used LST from GOES-R satellite (GOES-16, 2 km spatial resolution) (Yu et al. 2008; GOES-R Algorithm Working Group and GOES-R Program office, 2018) which provides hourly LST since December 2017. We extracted GOES-R LST for the grid cell in which each site was located, and used two years of data (2018

and 2019) for training. MODIS LST from Terra and Aqua was not considered because these two satellites together only provide four observations per day and cannot well sample the diurnal variation of LST. The land cover type, half-hourly SW and VPD from AmeriFlux sites that overlap the GOES-R observations (2018 and 2019) were used. For each site, we used the ReddyProc software (Wutzler et al. 2018) for the gap filling of EC data and partitioning of NEE into GPP and ecosystem respiration with the nighttime partitioning method (Reichstein et al. 2005). For each flux site, we extracted the daily MODIS bidirectional reflectance distribution function (BRDF)-corrected reflectance product MCD43A4 (Collection 6, 500 m) from MODIS and VIIRS Land Products Global Subsetting and Visualization Tool (ORNL DAAC 2018). The daily EVI was calculated from surface reflectances in near-infrared, red, and blue bands of the MCD43A4 and annual mean EVI was aggregated from the daily EVI. The machine learning approach can handle these different types of variables directly and normalizing these variables would not significantly influence the performance of the predictive model.

Flux tower data were obtained from the AmeriFlux website (https://ameriflux.lbl.gov). We identified AmeriFlux sites that had good-quality measurements available for the ECOSTRESS era and were also relatively homogeneous. For a given site, it was considered as relatively homogeneous if the dominant land cover type within the 1 km × 1 km area surrounding the site was consistent with the land cover type of the site. The 30-m NLCD land cover map was used to identify the land cover type for each grid cell. Heterogeneous sites were excluded from this analysis. A total of 56 AmeriFlux sites (containing 10 California sites) were used in this study, generating a dataset with a large number of hourly samples (165.1 thousand) encompassing a variety of climate and ecological conditions and ecosystem types across the U.S. We randomly used two thirds of the data points as training samples, and the remaining one third as testing data.

The details of AmeriFlux sites including site code, site name, location and biome were described in Table S2. The data sets used for training and prediction were summarized in Table 1.

Table 1. List of data for training and prediction

	Training			Prediction		
Variables	**Product**	**Spatial resolution**	**Temporal resolution**	**Product**	**Spatial resolution**	**Temporal resolution**
LST	GOES-R	~2 km	Hourly	ECOSTRESS	70 m	Instantaneous
SW	AmeriFlux	/	Half-hourly	ERA5	0.25°	Hourly
VPD	AmeriFlux	/	Half-hourly	ERA5	0.25°	Hourly
Land Cover	AmeriFlux	/	/	NLCD	30 m	/
EVI	MCD43A4	500 m	Daily	MCD43A4	500 m	Daily

2. 3. ECOSTRESS LST and other explanatory data for prediction

When the Cubist model was trained based on site-level samples, we then applied it with spatially explicit (i.e., 2D gridded) input data (Table 1) including ECOSTRESS LST, MODIS daily EVI and annual mean EVI, ERA5 hourly SW and VPD, and land cover from the NLCD to produce multiple 70 m, instantaneous GPP maps for four ecoregions across California.

Instantaneous ECOSTRESS LST was obtained from the Level-2 product - ECO2LSTE (Version 1), which provides both LST and emissivity retrieved from five thermal bands at a spatial resolution of ~70×70 m with the physics-based Temperature Emissivity Separation (TES) algorithm (Hulley and Hook 2010). Recent studies have shown that LST from ECOSTRESS was comparable to that from the existing thermal infrared instruments (Silvestri et al., 2020), and has high agreement with ground observations during the daytime (Li et al., 2020). The daily MODIS EVI throughout 2019 covering the study area were used to derive the annual mean EVI, which was used together with daily EVI corresponding to the ECOSTRESS overpass days for predicting the GPP. Both regional ECOSTRESS LST and EVI were retrieved using the Application for Extracting and Exploring Analysis Ready Samples (AppEEARS) online portal (AppEEARS

252 Team). The hourly SW and VPD corresponding to the ECOSTRESS overpass hours were obtained
253 from ERA5 reanalysis dataset (Hersbach and Dee 2016). For example, if ECOSTRESS overpassed
254 California around 14:20, the hourly SW and VPD starting from 14:00 to 15:00 were used to
255 represent the corresponding radiation and atmospheric water conditions. ERA5 is the latest
256 generation of global atmospheric reanalysis released by European Centre for Medium-Range
257 Weather Forecasts (ECMWF). ERA5 data on single levels contain a variety of hourly
258 meteorological variables at a horizontal resolution of $0.25^{\circ} \times 0.25^{\circ}$ from 1979 to present. The VPD
259 was calculated by the ERA5 2 m dewpoint temperature and 2 m air temperature. The land cover
260 type was identified by the land cover product from NLCD 2016 recently released by U.S.
261 Geological Survey (Yang et al. 2018). The NLCD land cover product was based on 30 m Landsat
262 imagery with cloud cover less than 20% and has an overall agreement with reference data from
263 71% to 97%.

264 The MODIS EVI and ERA5 meteorological data were resampled to 70 m resolution to match
265 the resolution of ECOSTRESS LST using the bilinear interpolation method. For each 70-m grid
266 cell, the land cover type was determined based on the nearest neighbor interpolation. Among these
267 input variables, the very coarse spatial resolution of ERA5 hourly data may affect the accuracy of
268 the GPP estimates. Therefore, we evaluated the hourly ERA5 SW and VPD against flux tower
269 data. Due to the very large number of hourly data points, we used the stratified sampling method
270 and evaluated the data for 24 hours in the first day of each month throughout 2018 for 44 sites with
271 flux data available. Across all sites, ERA5 hourly SW (R^2=0.90, RMSE=89.18 W m^{-2}) and VPD
272 (R^2=0.79, RMSE=4.34 hPa) were strongly correlated with tower measurements (Fig. S2a, b); at
273 the site level, ERA5 SW and VPD were also strongly related to tower data for the majority of the
274 sites (Fig. S2c, d). We also averaged hourly SW and VPD for 12 months for each site and found

that the site-averaged ERA5 hourly SW and VPD were also highly correlated with tower-averaged SW and VPD, respectively (R^2=0.97, RMSE=45.53 W m^{-2} for SW and R^2=0.75, RMSE=3. 47 hPa for VPD; Fig. S3). Therefore, the accuracy of the ERA5 SW and VPD data was reasonable.

2. 4. Evaluation of ECOSTRESS GPP and analysis of diurnal cycles

We first produced multiple 70-m resolution, instantaneous GPP maps for the central and northern California to examine the diurnal cycle of photosynthesis across biomes. We generated a total of nine images at different times of day during the summer from June to August 2019: 5:48 am, 8:37 am, 9:51 am, 10:43 am, 12:15 pm, 1:54 pm, 3:32 pm, 6:01 pm, and 7:43 pm local time. The acquisition time of the ECOSTRESS images was irregular because the instrument is aboard the ISS with an inclined, precessing orbit. These nine images could generally describe the changes in photosynthesis of vegetation over the course of one summer day. We then calculated regional averages of GPP for major biomes including deciduous forest, evergreen forest, mixed forest, cropland, wetland, shrubland and grassland to examine how the diurnal variations of photosynthesis varied across biomes.

We compared the spatial pattern of ECOSTRESS GPP with those of midday SIF from the Orbiting Carbon Observatory-2 (OCO-2) and TROPOspheric Monitoring Instrument (TROPOMI). The SIF has proven as a strong proxy of photosynthesis (Li et al. 2018), and therefore the consistency in spatial patterns between ECOSTRESS GPP and SIF based on qualitative evaluation can support the effectiveness of ECOSTRESS GPP and also highlight its higher spatial resolution. We compared our ECOSTRESS GPP at 1:54 pm, August 21, with SIF maps from TROPOMI (~12:10 pm, August 21) (Köhler et al. 2018) and OCO-2 (~12:55 pm) (Frankenberg et al. 2014). The OCO-2 SIF was aggregated over the interval from June to August 2019 due to the lack of OCO-2 overpass on the same day and the sparse coverage of OCO-2. It should be noted that the

298 difference in the overpass time between ECOSTRESS and OCO-2/TROPOMI could lead to
299 significant difference in the instantaneous photosynthetic activity as indicated by GPP and SIF.
300 We evaluated ECOSTRESS based GPP estimates for eight flux sites in California (Table 2).
301 The LST data for all the ECOSTRESS overpasses over each site from 2018 to 2019 were retrieved
302 using the AppEEARS tool. We compared the extracted LST for the grid cell where each site was
303 located and averaged LST from the neighboring pixels including 5 × 5, 10 × 10, and 15 × 15
304 windows surrounding the site (i.e., ~350 m to 1050 m away from the tower site) (Fig. S4). The
305 difference in LST (RMSE) between the grid cell and the average from different windows was
306 negligible and only slightly increased with window size, suggesting relatively homogeneous
307 temperature conditions within the ~1 km × 1 km window surrounding each site. Only cloud-free
308 LST indicated by the L2 cloud mask product (ECO2CLD.001) was then used to predict GPP.
309 ECOSTRESS does not provide its own cloud shadow layer. Since the Cubist model was
310 constructed based on LST from GOES-R, we compared GOES-R LST with the ECOSTRESS LST
311 for each site, and examined whether their difference would affect the GPP estimates.
312 For four sites with different land cover types including US-Ton (Tonzi Ranch, woody
313 savannas), US-Tw5 (East Pond Wetland, wetland), US-Bi1 (Bouldin Island Alfalfa, cropland), and
314 US-Snf (Sherman Barn, grassland), we further evaluated whether ECOSTRESS GPP could capture
315 the diurnal cycle of tower based GPP. Such analysis could only be conducted by pooling together
316 all the ECOSTRESS overpasses within a long temporal window, such as one month or whole
317 summertime, regardless of specific day because ECOSTRESS cannot provide temporally dense
318 observations in one day or one week. Therefore, we predicted GPP at different times of day in
319 August 2018 for the three sites (US-Ton, US-Bi1, US-Tw5), and compared them with mean hourly
320 tower GPP of August 2018. For US-Snf, we compared the predicted GPP and tower GPP at

different times of day during June to July 2019 because there were few ECOSTRESS overpasses in August 2018.

For the two cropland sites - US-Bi1 (Bouldin Alfalfa) and US-Bi2 (Bouldin Corn), ECOSTRESS had dense observations during the phenological transition period of vegetation which offers a valuable opportunity to examine whether ECOSTRESS-based GPP estimates could track the change in diurnal cycle resulted from seasonal dynamics of vegetation phenology. We predicted GPP for US-Bi1 in two periods: day of year (DOY) 152-171 and DOY 275-305 in 2019. The first period includes the cutting and regrowth dates during the alfalfa growing season which has multiple and periodical harvesting across the year. The second period is the senescence stage of alfalfa in late autumn. For US-Bi2, we predicted GPP for the early ("green-up") stage of the growing season (DOY 145-171 in 2019). The year 2018 was selected for examining the diurnal cycle for above four sites due to the availability of a number of ECOSTRESS overpasses, and the year 2019 was selected for examining the seasonal dynamics because ECOSTRESS provided continuous data from May to December 2019 while only about three months of data from July to mid-September were collected in 2018.

Finally, we produced another group of instantaneous GPP maps for two times in different seasons: one was around midday and the other one was afternoon, which helped us examine whether ECOSTRESS GPP could also capture the seasonal variations of photosynthesis at the regional scale. Four GPP maps around midday in 2019 were generated: 12:53 pm (June 6), 12:15 pm (August 25), 12:39 pm (October 5), and 11:01 am (December 6), and other four images in the afternoon were acquired: 4:14 pm (May 30), 3:32 pm (August 17), 3:05 pm (October 17), and 3:36 pm (December 16). The selected four maps for both times were used to represent four different seasons: early summer, summer, autumn, and winter, respectively. We did not generate GPP maps

344 for spring 2019 because ECOSTRESS data were not available due to the issues with the
345 ECOSTRESS recorders.

346 **3. Results**

347 *3.1. Model evaluation*

348 Using six explanatory variables (LST, SW, VPD, EVI, annual mean EVI, and land cover
349 type), we used the training dataset to develop the Cubist model, and found that Cubist performed
350 well to develop the predictive GPP model (RE=0.24, MAE= 1.22 μmol CO_2 m^{-2} s^{-1}, R=0.94). We
351 then used the testing tower GPP data to evaluate the performance of the model. The scatterplots
352 between half-hourly tower GPP and predicted GPP were shown in Fig. 4. Our model estimated
353 half-hourly GPP fairly well (R^2= 0.88, RMSE = 2.42 μmol CO_2 m^{-2} s^{-1}), and only slightly
354 underestimated GPP greater than 20 μmol CO_2 m^{-2} s^{-1} (Fig. 4a). The performance of the predictive
355 GPP model was consistently strong across biomes (Fig. 4b-i). Across the eight biomes, R^2 ranged
356 from 0.80 to 0.90, and RMSE ranged from 0.82 to 4.24 μmol CO_2 m^{-2} s^{-1}), indicating that our data-
357 driven approach driven by ECOSTRESS LST and other input data could estimate instantaneous
358 GPP fairly well for all the biomes.
359

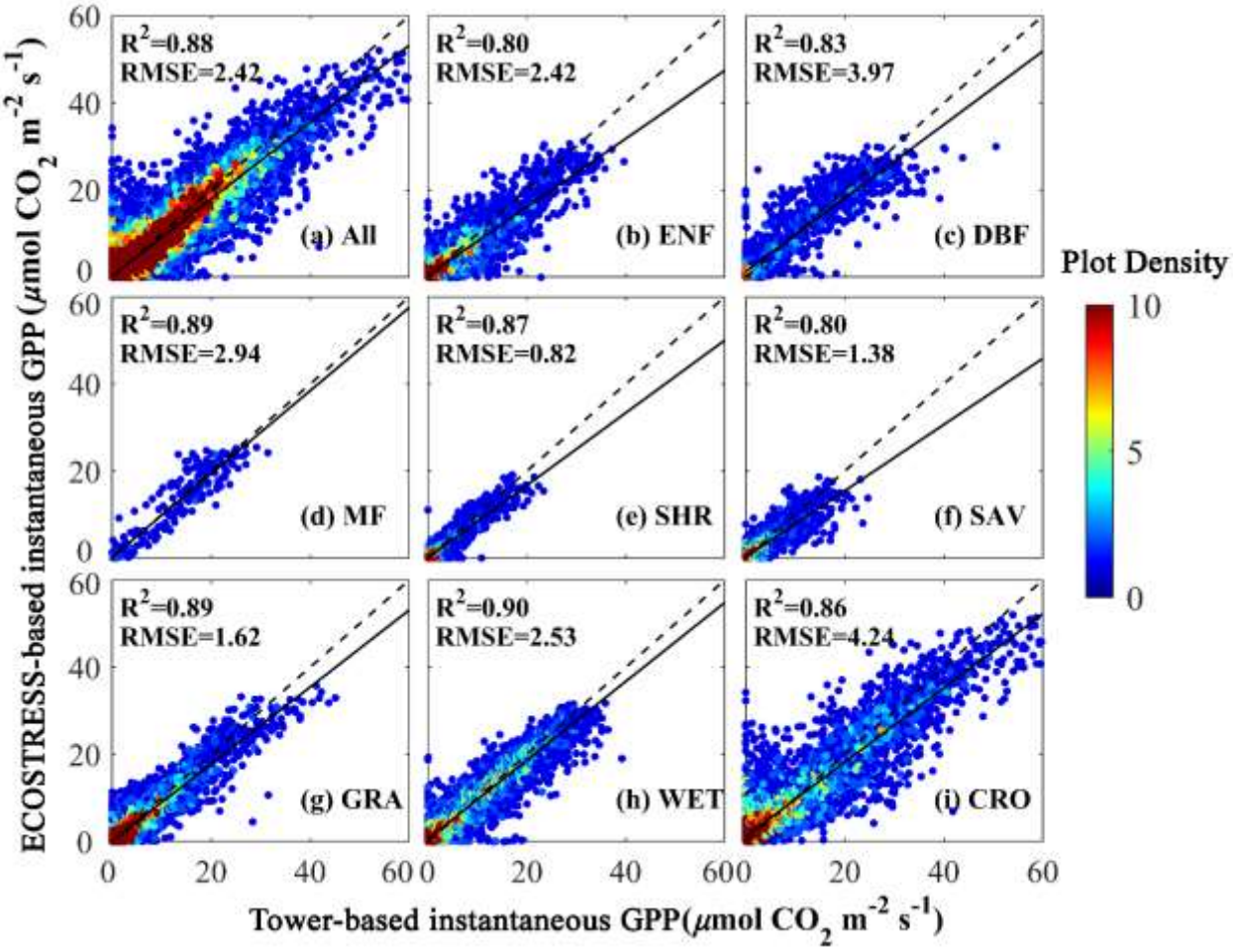

360

361 **Fig. 4.** The evaluation of the predictive model for the estimation of instantaneous GPP. (a) shows the
362 scatterplot of observed GPP versus predicted GPP by ECOSTRESS for all the testing data (y=0.88x+0.33);
363 (b-i) show the results separated by eight major biomes including evergreen needleleaf forests (ENF),
364 deciduous broadleaf forests (DBF), mixed forests (MF), shrublands (SHR), savannas (SAV), grasslands
365 (GRA), croplands (CRO), and wetlands (WET). All the relationships are statistically significant ($p <$
366 0.0001). The units of the RMSE are μmol CO_2 m^{-2} s^{-1}. The dashed line is the 1:1 line, and the solid line is
367 the regression line.

368 *3.2. Diurnal variations of ECOSTRESS GPP across California*

369 Fig. 5 shows the regional-scale diurnal variations in photosynthetic activity for four California
370 ecoregions in summer. Plants started photosynthesis at sunrise when the solar radiation was
371 available (Fig. 5a). The GPP increased in the morning (Fig. 5b-d) with plenty of sunlight and

favorable temperature and moisture conditions, and then peaked around midday (Fig. 5e, f). In the afternoon, the GPP began to decrease, and photosynthesis considerably slowed down and approached zero after sunset without sunlight (Fig. 5g-i).

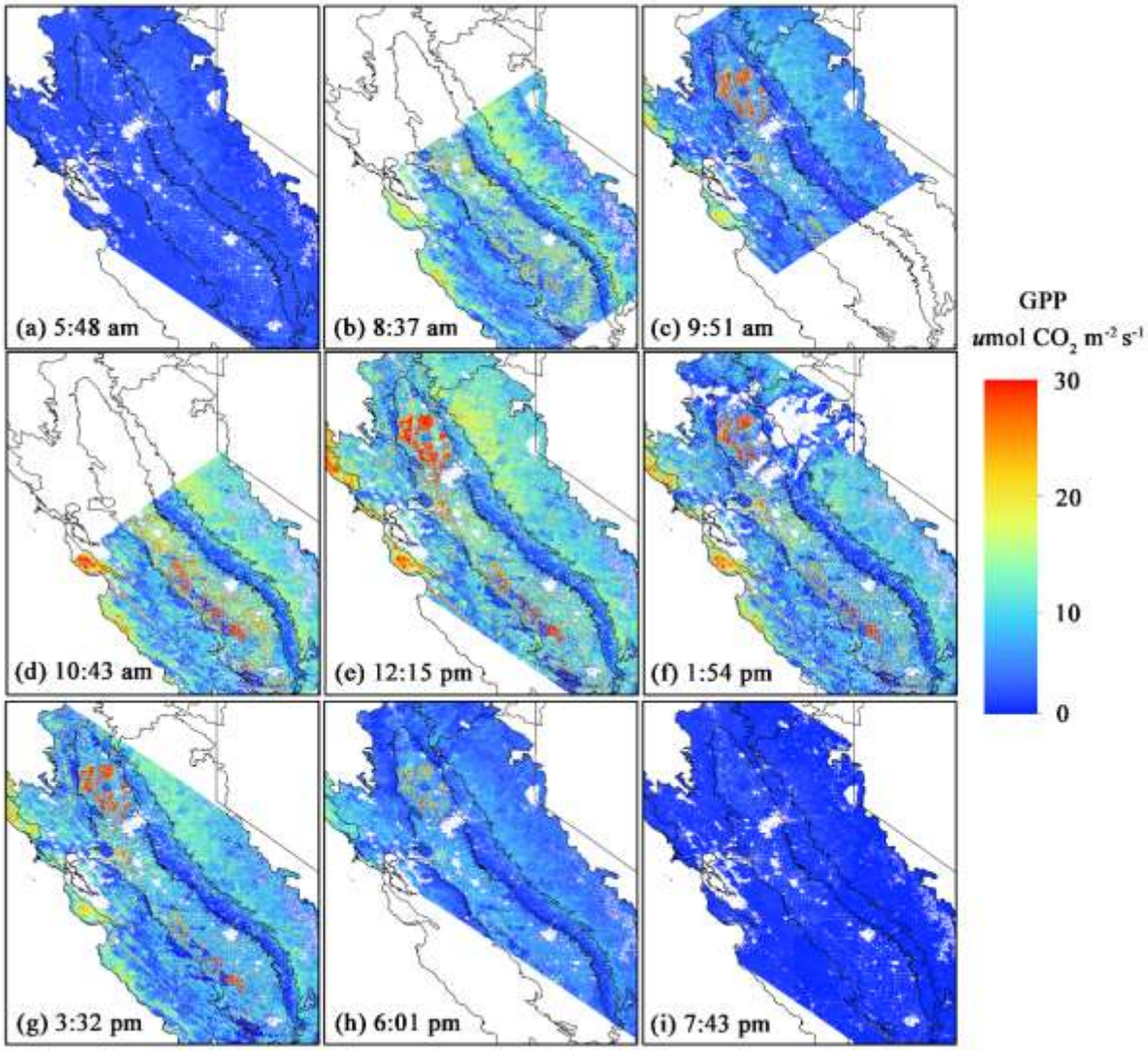

Fig. 5. Magnitude and spatial patterns of predicted ECOSTRESS GPP at different times of day in summer 2019 across the Central Foothills and Coastal Mountains, Central Valley, Sierra Nevada and Coast Range in California.

Fig. 5 also distinguishes the change in magnitude of photosynthesis for different biomes over the course of the day, and well captures the spatial variation of photosynthesis across different

ecoregions. The forests located in Coast Range and western Sierra Nevada (higher latitude) and croplands in Central California Valley had high productivity during the daytime (Fig. 5b-h). This was in stark contrast to the woodlands and grasslands in Central California Foothills and Coastal Mountains which had consistently lower photosynthesis (less than 10 *u*mol CO_2 m^{-2} s^{-1}) throughout the day. The croplands with the highest photosynthetic capacity were also highlighted, which had particularly high GPP values (more than 30 *u*mol CO_2 m^{-2} s^{-1}) from morning to early afternoon (Fig. 5c-g), and still maintained moderate GPP value around 20 *u*mol CO_2 m^{-2} s^{-1} in the late afternoon (Fig. 5h). These highly productive croplands mainly include rice in northwestern Central Valley and cotton in southeastern Central Valley. We also averaged regional GPP for each major biome for these nine images at different times (Fig. 6). The regionally averaged ECOSTRESS GPP showed clear diurnal variations for all the biomes. Forests, cropland, and wetland had higher GPP than shrubland and grassland throughout the day. Among forests, evergreen forest had the highest productivity, followed by mixed forest and deciduous forest.

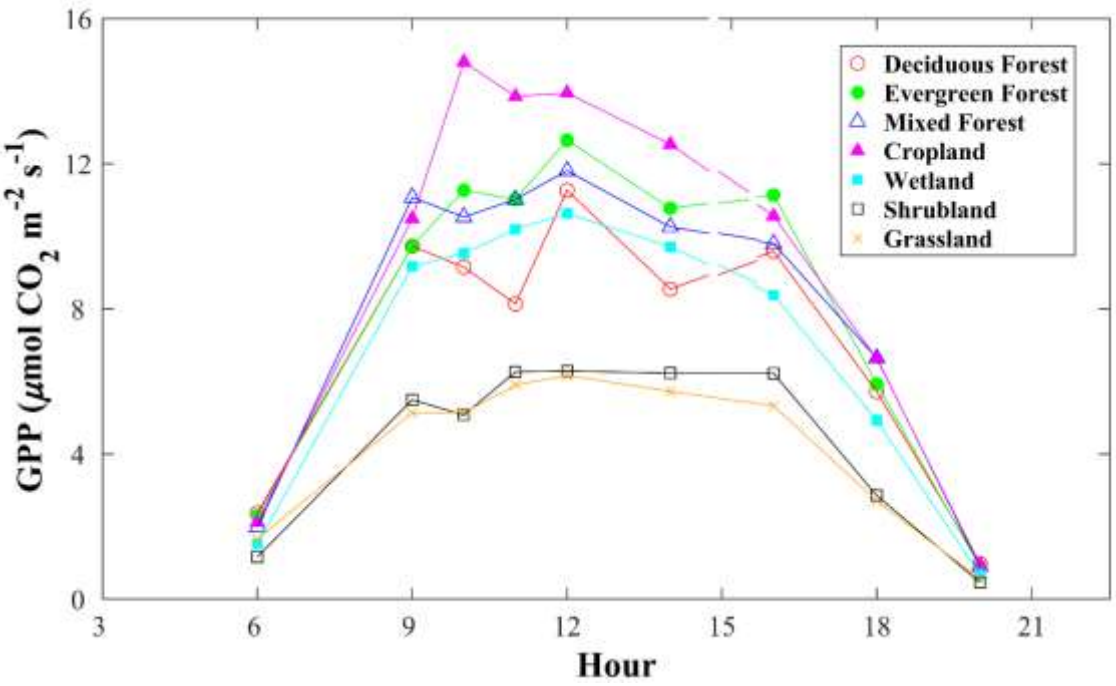

Fig. 6. Diurnal cycles of predicted ECOSTRESS GPP ($u$mol CO_2 m^{-2} s^{-1}) for the major biomes including deciduous forest, evergreen forest, mixed forest, cropland, wetland, shrubland and grassland.

ECOSTRESS-based GPP estimates exhibited overall consistent spatial pattern with SIF from OCO-2 and TROPOMI (Fig. 7). Compared with the two SIF maps, ECOSTRESS GPP had spatially continuous coverage, and could also provide much more spatial details, which allows for examining photosynthesis at an individual field level and provides more accurate characterization for the transition zones between different ecoregions. Although ECOSTRESS GPP exhibited overall consistent spatial pattern with SIF from OCO-2 and TROPOMI, SIF indicated higher photosynthetic capacity for croplands in the southeastern Central Valley relative to other biomes than did GPP. This is likely due to the fact that the ecosystems in California tend to have the highest photosynthetic activity around noon, while the overpass time of OCO-2 (~1:55 pm) and TROPOMI (~12:10 pm) was ~1 hour and ~1.7 hour earlier than that of ECOSTRESS (1:54 pm). More importantly, ECOSTRESS-based GPP could provide GPP estimates for different times of day, while OCO-2 and TROPOMI only provide SIF snapshots for the same time of day.

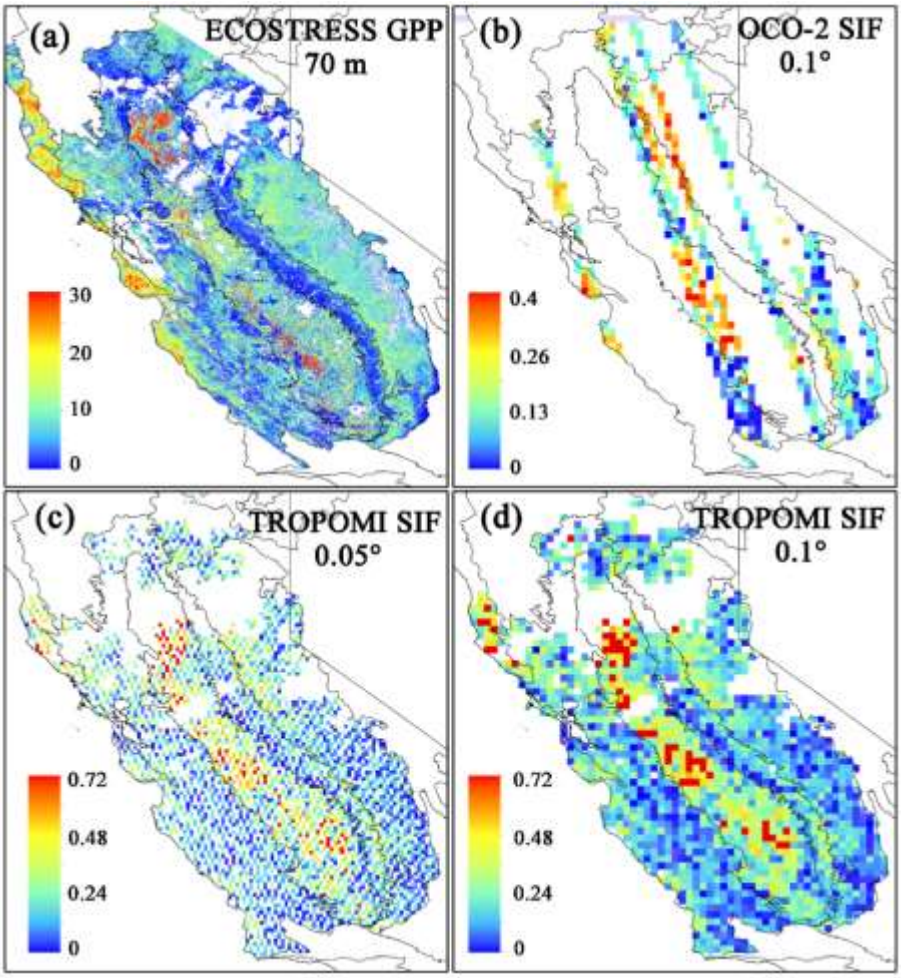

411

412 **Fig. 7.** Spatial patterns of predicted ECOSTRESS GPP (70 m) at 1:54 pm on August 21, 2019 (a), OCO-2
413 SIF (0.1°) at ~12:55 pm aggregated from June to August 2019 (b), and TROPOMI SIF at ~12:10 pm on
414 August 21, 2019 (c: 0.05°; d: 0.1°) across California. TROPOMI (740 nm) has higher SIF signal than OCO-
415 2 (757 nm). The units of GPP and SIF are μmol CO_2 m^{-2} s^{-1} and W m^{-2} μm^{-1} sr^{-1}, respectively. Please note
416 that the difference (~1 hour for ECOSTRESS versus OCO-2 and ~1.7 hour for ECOSTRESS versus
417 TROPOMI) in overpass time between ECOSTRESS and OCO2/TROPOMI can lead to significant
418 differences in the spatial patterns between instantaneous GPP and instantaneous SIF.

419 *3.3. Diurnal variations of ECOSTRESS GPP at the site level*

420 The predicted GPP driven by ECOSTRESS LST was highly correlated with tower GPP for
421 most of the sites (R^2=0.53–0.96, Table 2). We also predicted GPP directly using LST from GOES-

R for the seven sites except for US-Snf, and found that the performance was very similar to that based on ECOSTRESS LST (two rightmost columns in Table 2). The LST from ECOSTRESS was strongly consistent with that from GOES-R (Fig. S4), although some differences were found for the US-Snf site that was surrounded by water within the footprints of GOES-R (2–3 km). This suggests that the temporal disagreement in LST between ECOSTRESS and GOES-R at the site level was negligible and GOES-R LST could be used for the training of the GPP model. ECOSTRESS GPP performed the best for cropland and wetland sites, while performed moderately for US-Var site which had smaller diurnal variation of GPP during the non-growing season.

Table 2. Evaluation of instantaneous ECOSTRESS GPP for the eddy covariance flux sites in California. N is the number of ECOSTRESS overpasses for each site; R^2_e and RMSE_e are the measures for GPP predictions driven by ECOSTRESS LST, while R^2_g and RMSE_g are the measures for GPP directly based on GOES-R LST. The units of RMSE are μmol CO_2 m^{-2} s^{-1}. The GOES-R LST was not used to predict GPP for the US-Snf site because US-Snf was surrounded by water within the footprint of GOES-R (2 km × 2 km). ECOSTRESS LST with much smaller footprint can better represent the temperature condition around this site.

Site ID	Lat	Lon	Biome	N	R^2_e	RMSE_e	R^2_g	RMSE_g
US-Bi1	38.10	-121.50	CRO	88	0.88	4.40	0.90	4.21
US-Bi2	38.11	-121.54	CRO	38	0.95	5.14	0.95	5.32
US-Snf	38.04	-121.73	GRA	45	0.71	4.59	/	/
US-Ton	38.43	-120.97	SAV	49	0.85	1.50	0.84	1.38
US-Tw1	38.11	-121.65	WET	87	0.96	1.96	0.95	2.10
US-Tw4	38.10	-121.64	WET	89	0.95	2.09	0.95	2.08
US-Tw5	38.11	-121.64	WET	76	0.99	1.10	0.99	1.10
US-Var	38.41	-120.95	GRA	53	0.53	1.97	0.60	1.76
All	/	/	/	/	0.91	3.02	0.91	2.99

Our predicted ECOSTRESS GPP was able to produce similar shapes of diurnal cycle of tower GPP for four flux sites with different land cover (Fig. 8). The time of onset, peak, and end of photosynthesis was well captured. US-Tw5 (wetland) and US-Bi1 (cropland) maintained high

photosynthetic activity for a long time during the day (e.g., 9 am- 4 pm), leading to relatively flat diurnal curve, especially near the peak. For US-Ton, a woody savanna site, photosynthesis peaked in the morning (about 10 am), and then decreased till the sunset. The ECOSTRESS GPP captured such two contrasting diurnal changes of photosynthesis fairly well, although it showed fluctuations for US-Bi1 (12:00 pm to 3 pm). For the grassland site - US-Snf (Fig. 8d), the ECOSTRESS GPP moderately overestimated the tower GPP, but it still showed consistent diurnal variation. Note that the large standard deviation of monthly averaged GPP for US-Bi1 resulted from a mix of high and low GPP as the leaf area index (LAI) of alfalfa changed quickly during the growing season (Fig. 8c).

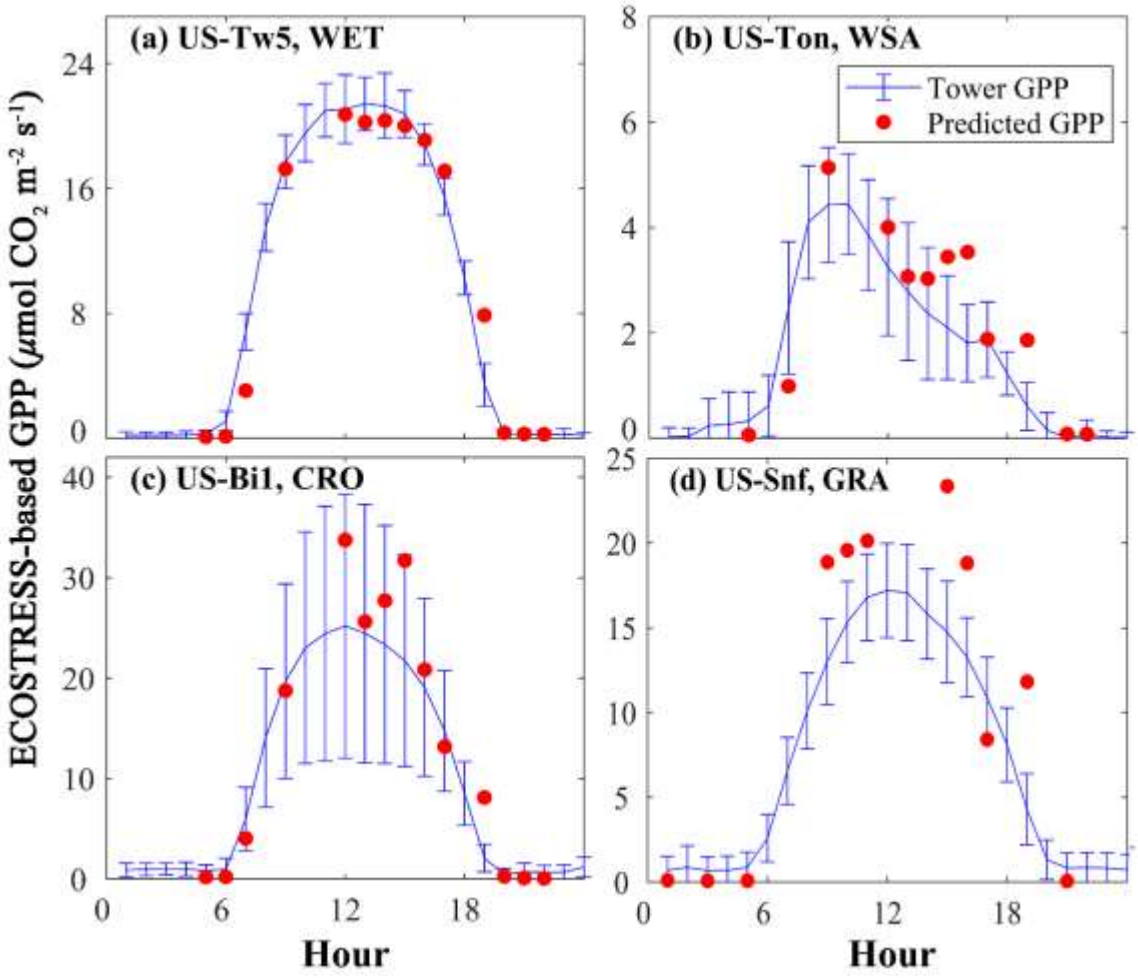

Fig. 8. Diurnal cycles of tower GPP and ECOSTRESS GPP for (a) US-Tw5, (b) US-Ton, (c) US-Bi1, (d) US-Snf. Blue curves denote averaged hourly tower GPP during August 2018 (a-c) and June to July 2019 (d); red circles denote estimated ECOSTRESS GPP. The predicted GPP was strongly correlated with tower GPP: US-Tw5 (R^2=0.99, p<0.0001, RMSE=1.1 μmol CO_2 m^{-2} s^{-1}), US-Ton (R^2=0.85, p<0.0001, RMSE=1.5 μmol CO_2 m^{-2} s^{-1}), US-Bi1 (R^2=0.88, p<0.0001, RMSE=4.4 μmol CO_2 m^{-2} s^{-1}),, and and US-Snf (R^2=0.71, p<0.0001, RMSE=4.59 μmol CO_2 m^{-2} s^{-1}) (Table 2).

3.4. Seasonal variations in diurnal cycling of ECOSTRESS GPP

The diurnal cycling of tower GPP varied with the seasonal growth of vegetation (Fig. 9). For example, at US-Bi2, the green-up of plants began around DOY 161 when the maximum GPP in the diurnal cycle significantly increased; the peak instantaneous GPP approached to about 15 *u*mol CO_2 m^{-2} s^{-1} on DOY 171 (Fig. 9a, b). For US-Bi1, GPP suddenly dropped from 30 *u*mol CO_2 m^{-2} s^{-1} on DOY 291 to near zero after DOY 292 during autumn senescence (Fig. 9c, d). The predicted ECOSTRESS GPP, although not temporally continuous, well tracked the trajectory of tower GPP in such two different phenological stages of plant growth.

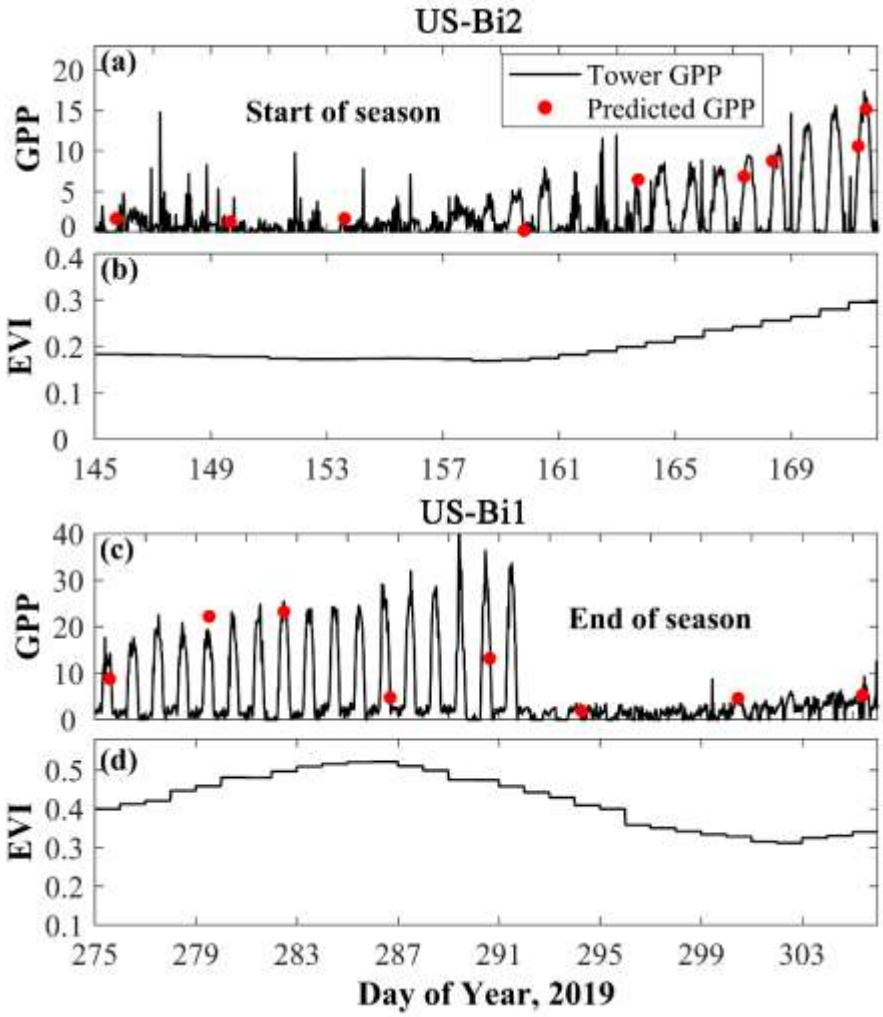

464

465 **Fig. 9.** Diurnal cycling of photosynthesis changes with plant phenology at the US-Bi1 and US-Bi2
466 sites. (a-b) show the dynamics of tower GPP, predicted ECOSTRESS GPP, and MODIS EVI during the
467 green-up of plants for US-Bi2; (c-d) show these three variables during the senescence of plants for US-
468 Bi1. Other sites were not included because there were very few or no ECOSTRESS overpasses during these
469 phenological stages in 2018 and 2019.

470 For the alfalfa site (US-Bi1), ECOSTRESS GPP captured the multiple and periodical
471 harvesting characteristic of alfalfa within one year (Fig. 10). The alfalfa had high productivity
472 during DOY 152-159; the maximum instantaneous GPP decreased to less than 5 $u$mol CO_2 m^{-2} s^{-1}
473 during the period DOY 160-165 from the harvest to the replanting of alfalfa, and then increased

during the next growth cycle (Fig. 10a). The cutting of alfalfa led to an increase in ambient temperature, which was revealed by both ECOSTRESS and GOES-R LST (Fig. 10b).

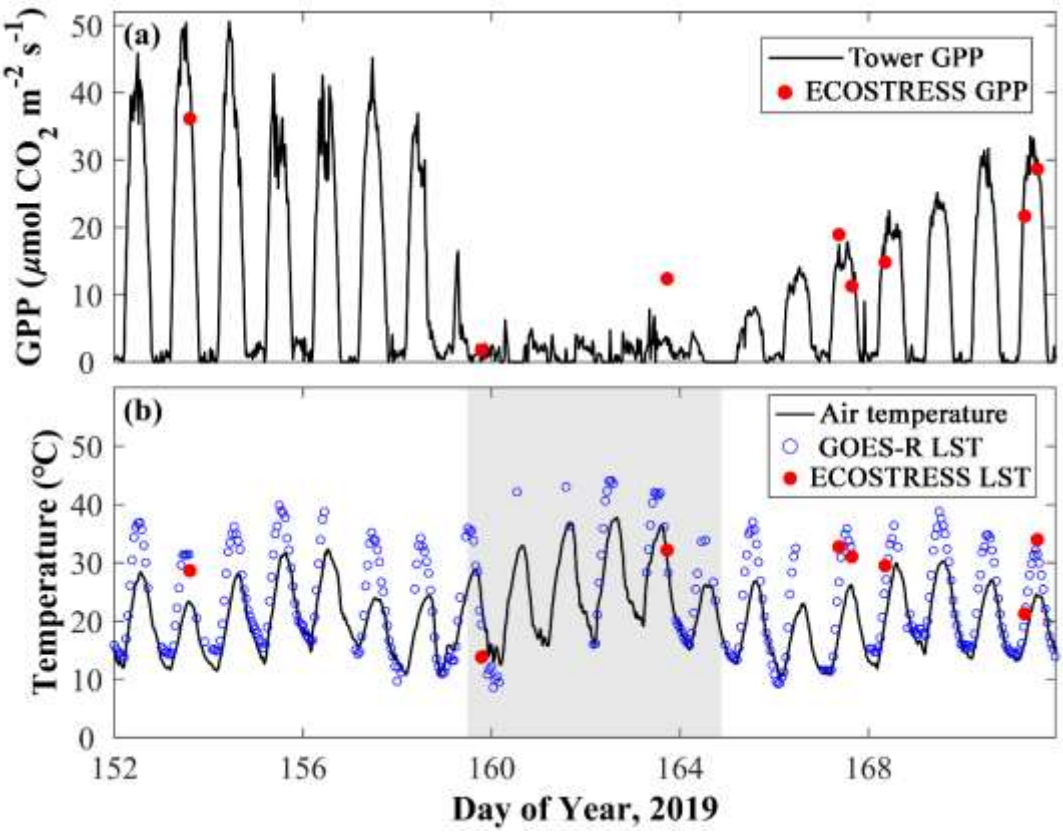

Fig. 10. Diurnal cycling of photosynthesis changes with the cutting and regrowth of alfalfa at the US-Bi1 site. (a) shows the dynamics of tower GPP and predicted ECOSTRESS GPP; (b) shows the changes in air temperature and land surface temperature. The shaded areas indicate the increase in temperature during the period from the harvest to the replanting of alfalfa. The predicted GPP on DOY 163 was much higher than tower GPP mainly because the 500-m MODIS EVI on that day contained information on the crop field in which the tower is located and neighboring fields that crops were not yet harvested.

Finally, we produced instantaneous GPP maps in different seasons to examine how instantaneous GPP varied with seasons. ECOSTRSS GPP exhibited clear seasonal variations at both midday and afternoon (Fig. 11). The majority of the grid cells showed high GPP in early summer and continued to increase by August. With the gradual senescence of plants, the GPP

showed small or intermediate values in the autumn and had the lowest values in winter due to the dormancy of deciduous plants. Evergreen forests in Sierra Nevada continued to conduct photosynthesis but with substantially reduced rates in the winter (Fig. 11 d and h).

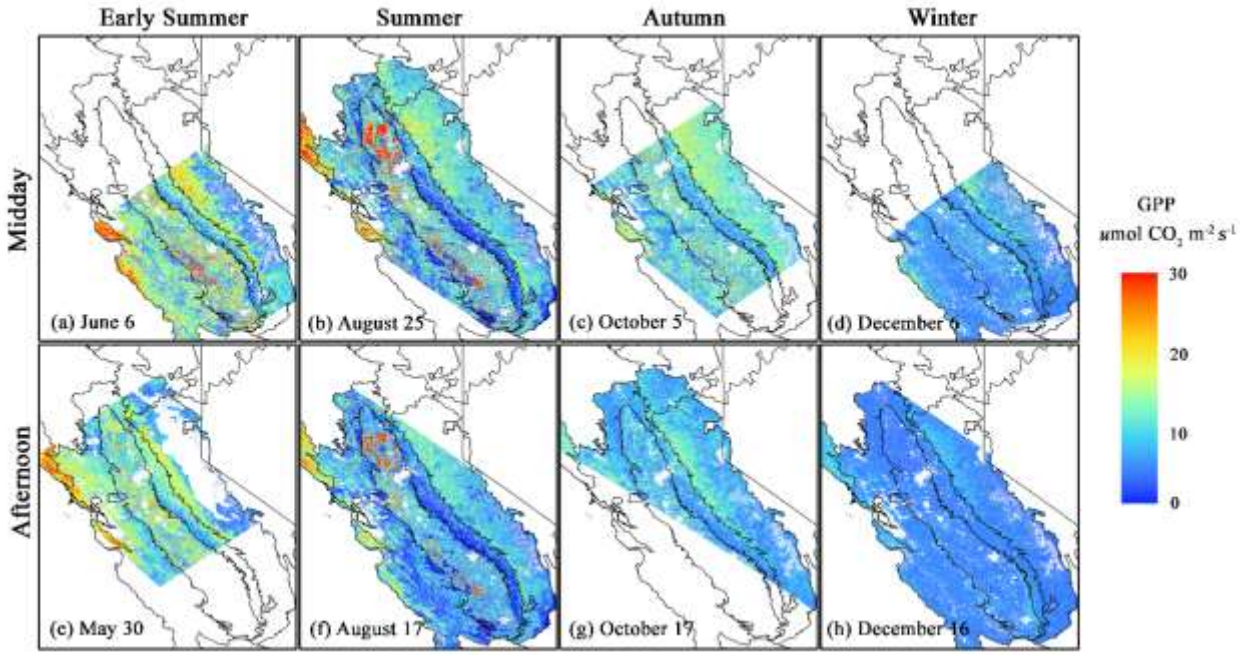

Fig. 11. Magnitude and spatial patterns of predicted ECOSTRESS GPP at midday (*upper panel*) and afternoon (*lower panel*) in early summer, summer, autumn, and winter across California.

4. Discussion

This study provides the first demonstration of using the new ECOSTRESS thermal observations for estimating instantaneous GPP over the course of the diurnal cycle at regional scales. Previous studies based on polar-orbiting satellites such as Landsat, Sentinel, Terra, Aqua, and OCO-2 can only estimate GPP at daily or 8-day time steps and coarse spatial resolutions (e.g., 1 km) (Running et al. 2004; Xiao et al. 2010; Zhao et al. 2005; Li and Xiao 2019a). The ECOSTRESS-based GPP estimates in this study have two significant advantages which raise previous approaches to the next level: (1) measuring the sub-daily variations in ecosystem photosynthesis at the large scale and has the potential to extend globally (between 53.6° N and

502 53.6° S); and (2) depicting these variations at a fine spatial resolution (70 m). These were realized
503 by an important variable LST provided by ECOSTRESS along with other vegetation and
504 instantaneous meteorological variables.

505 The ECOSTRESS-based GPP estimates well characterized the changes in photosynthetic
506 activity over the course of the diurnal cycle across different ecoregions in California. The diurnal
507 variations in GPP were driven by environmental (e.g., solar radiation, air temperature, soil
508 moisture, VPD) and physiological (e.g., stomatal conductance) factors (Damm et al. 2010; Franco
509 and Lüttge 2002; Paul-Limoges et al. 2018). LST measures skin temperature of the surface
510 including soil temperature for bare soil and canopy temperature for vegetation, and is a more useful
511 measure of physiological activity of canopy leaves than air temperature (Sims et al. 2008). LST
512 measured by ECOSTRESS has high spatial resolution (i.e., 70m) at different times of day, and is
513 also physiologically related to plant photosynthesis. Specifically, both low and high temperature
514 will affect the enzyme activity (e.g., Rubisco) and intercellular CO_2 concentration that underlie the
515 photosynthesis process (Ferrar et al. 1989; Fredeen and Sage 1999, Allen and Ort 2001). High
516 temperature will even lead to a reduction of stomatal conductance to prevent further loss of water
517 through transpiration, but at the expense of reduced photosynthesis (Ferrar et al. 1989; Xu et al.
518 2020).

519 The diurnal amplitude of predicted GPP varied with ecosystems. Parts of the croplands with
520 the highest instantaneous productivity were highlighted by ECOSTRESS GPP maps, which was
521 consistent with the recent study that also reported the maximum GPP of some croplands during
522 the day across the globe (Bodesheim et al. 2018). Shrubland and grassland had lower productivity
523 due to their low vegetation cover or LAI. Tower-based GPP confirmed this wide range of
524 photosynthetic capacity across biomes, indicating that our model was adept at simulating the highs

and the lows. The predicted GPP, although produced at the sub-daily time scale, could also indicate the seasonal growth of plants. Plants experience large changes in vegetation structure (e.g., LAI or the absorbed fraction of photosynthetically active radiation, *f*PAR) during the critical phenological transition dates (e.g., start or end of growing season), which can cause apparent changes in productivity. For the harvesting of alfalfa, the cutting could also lead to the increase of ambient temperature. The proper use of predictor variables in our model including ECOSTRESS LST, vegetation, and environmental variables is essential for ensuring the consistency between estimated and tower GPP.

The ECOSTRESS GPP enables the examination of instantaneous physiological variations of plants in response to environmental conditions, such as high temperature, excessive radiation, and water stress. These important physiological characteristics would be easily obscured when analyses were conducted at daily or monthly scales. Our predicted ECOSTRESS GPP successfully produced the different shapes of diurnal courses which were in line with corresponding tower GPP. The "midday depression" phenomenon was observed at the woody savanna site - US-Ton (Fig. 8), which indicated the distinct reduction in GPP (or carbon exchange) at midday. This phenomenon was caused by high temperature and high VPD that was often linked to limited water supply (Damm et al. 2010), which led to the closure of stomata to conserve water at the expense of reduced carbon uptake. The midday depression was discussed by previous studies based on in situ observations (Damm et al. 2010; Lin et al. 2019a; Liu et al. 2017; Paul-Limoges et al. 2018), and found for different ecosystems such as grassland, mixed forest, and cropland (Damm et al. 2010; Paul-Limoges et al. 2018; Wagle and Kakani 2014). Fig. S6 showed that the decrease of GPP at the US-Ton site was followed by the peak of incoming radiation, with progressive increase of air temperature and VPD from midday to 4 pm. The midday depression was not found for other

three sites with lower temperature and atmospheric water stresses. The response of photosynthesis to temperature was confounded by the covariations in light intensity, air dryness, and soil moisture across biomes (Ma et al. 2017).

Our study well demonstrates the feasibility of using ECOSTRESS observations for predicting instantaneous GPP and the ability of ECOSTRESS based GPP estimates for examining the variations in photosynthesis over the course of the diurnal cycle at regional scales. This method can also be extended to other regions or even the globe encompassing various climatic conditions and ecosystem types. When the global ECOSTRESS GPP covering one or two years is available in the near future, it will undoubtedly make great contributions to the scientific community. The regional to global ECOSTRESS GPP will be valuable for various ecological studies. For example, it can indicate what time of the day plants "wake up" to begin photosynthesis and what time of the day they “sleep” and stop photosynthesis from space. The ECOSTRESS GPP can help scientists understand how plants absorb carbon dioxide over the course of the day, how the magnitude and shape of diurnal course vary across latitude, plant species, and climatic zones, and how temperature and water stresses influence photosynthesis throughout the day. The instantaneous ECOSTRESS GPP is also essential for monitoring the water use efficiency (WUE) of plant throughout the day, which partly inspired our research in this study. Combined with the instantaneous ECOSTRESS ET (L3 product) (Fisher et al. 2015), ECOSTRESS GPP can generate ‘real’ instantaneous WUE estimates, and help better address the scientific questions of the ECOSTRESS mission. With these products, scientists may better understand how plants use water for carbon uptake and identify critical thresholds of water use and water stress in climate-sensitive biomes globally. These instantaneous products have great potential for informing agricultural irrigation management. For example, farmers can adjust the timing and location for crop irrigation. It also helps improve the

ability of agricultural drought monitoring and can point out which areas and which biomes are more susceptible to drought. ECOSTRESS GPP for different times of day will also be valuable for benchmarking terrestrial biosphere models and Earth system models such as the Community Land Model (CLM) (Lawrence et al. 2019) at the diurnal timescales.

The combination of high-resolution ECOSTRESS LST (70 m), medium-resolution MODIS EVI (500 m), and much coarser ERA5 meteorological data (0.25º) in this study estimated GPP effectively for different times of day. For a given ECOSTRESS grid cell, the corresponding 500 m MODIS EVI can contain information on not only the ECOSTRESS grid cell but also neighboring grid cells that may have different productivity, vegetation type, or phenology, likely leading to over- or under-estimation of GPP. In future work, finer-resolution EVI data from Landsat or Sentinel should be used to improve the accuracy of GPP. The overall match of EAR5 with tower measurements (Fig. S2-3) showed that the use of coarse-resolution ERA5 data had relatively small effects on the accuracy of GPP. However, ERA5 data were simply interpolated to 70-m resolution with a bilinear interpolation approach, and as a result, the "true" spatial resolution of the resulting GPP estimates is coarser than 70 m. Future work could benefit from downscaling EAR5 with a better strategy. A potential strategy is to merge ERA5 with Daymet (https://daymet.ornl.gov), a daily, gridded meteorological dataset with 1-km spatial resolution, to generate a new dataset with hourly time step and 1-km spatial resolution. The hourly meteorological data with much finer resolution (e.g., 1 km) and EVI data with fine resolution (e.g., 30-70 m) could enhance the spatial details and ensure the fine spatial resolution of ECOSTRESS GPP.

Despite the great potential, the ECOSTRESS GPP enables the monitoring of diurnal changes of photosynthesis by pooling together the observations at different times of day in multiple days

(unusually longer than half a month), which is inherently limited by the overpass of ECOSTRESS. The variations in instantaneous GPP over such a period can be caused by not only the diurnal variations in photosynthesis but also day-to-day variations resulting from day-to-day changes in environmental factors (e.g., meteorological variables), LAI, and phenology, which will likely complicate the analyses of diurnal variations. As mentioned earlier, the geostationary satellites (e.g., GOES-R, Himawari-8) can provide temporally dense observations within one day but with a coarse spatial resolution. High-frequency GEOS-R LST data have recently been used to study the diurnal cycling of surface urban heat island in Boston (Chang et al. 2021). Synergistic use (i.e., data fusion) of LST from ECOSTRESS and geostationary satellites have the potential to maintain high resolution in both time and space and thereby better monitor the diurnal changes of photosynthesis. The combination of ECOSTRESS data with Landsat observations or thermal infrared spaceborne measurements from upcoming missions such as the Surface Biology and Geology (SBG) designated observable and Land Surface Temperature Monitoring (LSTM) mission from the European Space Agency (ESA) is also likely to produce more temporally dense images for better monitoring of plant photosynthesis.

5. Conclusions

This study is the first attempt to produce instantaneous GPP maps with fine spatial resolution (70 m) for different times of day using ECOSTRESS observations and to use the instantaneous GPP maps to examine the diurnal variations of photosynthesis across biomes at the regional scale. We used the instantaneous LST from ECOSTRESS, vegetation index from MODIS, hourly meteorological variables from ERA5, and land cover from the NLCD dataset along with a data-driven (or machine learning) method to predict instantaneous GPP. The predictive GPP model performed well for different biomes, with R^2 ranging from 0.80 to 0.90, and RSME from 0.82 to

617 4.24 μmol CO_2 m^{-2} s^{-1}. The predicted ECOSTRESS GPP maps well captured the variations of
618 photosynthesis over the course of the diurnal cycle, and clearly depicted the differences in
619 photosynthetic capacity for different biomes throughout the day. The ECOSTRESS GPP also
620 indicated the varying photosynthesis of plants during key phenological transition periods. Future
621 work is needed to increase the temporal density of the instantaneous GPP estimates for different
622 times of day with more frequent satellite data (e.g., geostationary satellites such as GOES-R and
623 Himawari-8) and to strengthen the spatial resolution of the GPP estimates with finer-resolution
624 EVI (e.g., Landsat, Sentinel) and meteorological reanalysis data. ECOSTRESS GPP will have
625 strong potential for ecological applications. It will be useful for understanding how plants absorb
626 carbon over the course of the diurnal cycle. In combination with instantaneous ECOSTRESS ET,
627 it will also allow us to how plants use water and how plant water use efficiency varies throughout
628 the day. ECOSTRESS GPP is also useful for benchmarking terrestrial biosphere and Earth system
629 models at diurnal timescales.
630
631 **Author Contributions**
632 X. Li and J. Xiao designed the research, conducted data analyses, and wrote the manuscript. J.B.
633 Fisher and D.B. Baldocchi contributed data and to the writing of the manuscript.
634
635 **Acknowledgements**
636 This study was supported by the National Aeronautics and Space Administration (NASA)
637 (ECOSTRESS Science and Applications Team: Grant No. 80NSSC20K0167) and the National
638 Science Foundation (NSF) (Macrosystem Biology & NEON-Enabled Science program: DEB-
639 2017870). JBF contributed to the research at the Jet Propulsion Laboratory, California Institute of
640 Technology, under a contract with NASA and with support from the ECOSTRESS mission and

R&A program. We thank Dr. Glynn Hulley for providing ECOSTRESS LST data and the OCO-2 and TROPOMI science teams for making OCO-2 SIF and TROPOMI SIF data available. We also acknowledge ECMWF and Copernicus Climate Change Service information for generating ERA5 data. We thank the AmeriFlux primary investigators for providing their data. Funding for AmeriFlux data resources was provided by the U.S. Department of Energy's Office of Science. The AρρEEARS tool was developed in collaboration with the following data repositories: the NASA, National Snow and Ice Data Center, Socioeconomic Data and Applications Center, Land Processes Distributed Active Archive Center, and Oak Ridge National Laboratory Distributed Active Archive Center. We thank the four anonymous reviewers for their constructive and insightful comments on the manuscript.

References

Allen, D.J., & Ort, D.R. (2001). Impacts of chilling temperatures on photosynthesis in warm-climate plants. Trends in Plant Science, 6, 36-42

Anderson, M.C., Norman, J.M., Mecikalski, J.R., Otkin, J.A., & Kustas, W.P. (2007). A climatological study of evapotranspiration and moisture stress across the continental United States based on thermal remote sensing: 1. Model formulation. *Journal of Geophysical Research: Atmospheres, 112*

AppEEARS Team. Application for Extracting and Exploring Analysis Ready Samples (AppEEARS). NASA EOSDIS Land Processes Distributed Active Archive Center (LP DAAC), USGS/Earth Resources Observation and Science (EROS) Center: Sioux Falls, SD, USA. Available online: https://lpdaacsvc.cr.usgs.gov/appeears/ (accessed on 19 January 2020).

Baldocchi, D., Dralle, D., Jiang, C., & Ryu, Y. (2019). How much water is evaporated across California? A multiyear assessment using a biophysical model forced with satellite remote sensing data. *Water Resources Research, 55*, 2722-2741

Baldocchi, D., Falge, E., Gu, L., Olson, R., Hollinger, D., Running, S., Anthoni, P., Bernhofer, C., Davis, K., & Evans, R. (2001). FLUXNET: A new tool to study the temporal and spatial variability of

668 ecosystem–scale carbon dioxide, water vapor, and energy flux densities. *Bulletin of the American*
669 *Meteorological Society, 82*, 2415-2434
670 Beer, C., Reichstein, M., Tomelleri, E., Ciais, P., Jung, M., Carvalhais, N., Rödenbeck, C., Arain, M.A.,
671 Baldocchi, D., & Bonan, G.B. (2010). Terrestrial gross carbon dioxide uptake: global distribution and
672 covariation with climate. *Science*, 1184984
673 Chang, Y., Xiao, J., Li, X., Frolking, S., Zhou, D., Schneider, A., Weng, Q., Yu, P., Wang, X., Li, X., Liu,
674 S., Wu, Y. (2021) Exploring diurnal cycles of surface urban heat island intensity in Boston with land
675 surface temperature data derived from GOES-R geostationary satellites. Science of the Total
676 Environment, 763, 144224. https://doi.org/10.1016/j.scitotenv.2020.144224.
677 Bodesheim, P., Jung, M., Gans, F., Mahecha, M.D., & Reichstein, M. (2018). Upscaled diurnal cycles of
678 land-atmosphere fluxes: a new global half-hourly data product. *Earth System Science Data, 10*, 1327-
679 1365
680 Damm, A., Elbers, J., Erler, A., Gioli, B., Hamdi, K., Hutjes, R., Kosvancova, M., Meroni, M., Miglietta,
681 F., & Moersch, A. (2010). Remote sensing of sun-induced fluorescence to improve modeling of diurnal
682 courses of gross primary production (GPP). *Global Change Biology, 16*, 171-186
683 Ferrar, P., Slatyer, R., & Vranjic, J. (1989). Photosynthetic temperature acclimation in Eucalyptus species
684 from diverse habitats, and a comparison with Nerium oleander. *Functional Plant Biology, 16*, 199-217
685 Fisher, J.B., Hook, S., Allen, R., Anderson, M., French, A.N., Hain, C., Hulley, G.C., & Wood, E.F. (2015).
686 ECOSTRESS: NASA's next-generation mission to measure evapotranspiration from the International
687 Space Station. In, *AGU Fall Meeting Abstratcs; AGU: Washington, DC, USA*
688 Fisher, J.B., Lee, B., Purdy, A.J., Halverson, G.H., Dohlen, M.B., Cawse-Nicholson, K., Wang, A.,
689 Anderson, R.G., Aragon, B., & Arain, M.A. (2020). ECOSTRESS: NASA's next generation mission
690 to measure evapotranspiration from the International Space Station. *Water Resources Research, 56*,
691 e2019WR026058
692 Fisher, J.B., Tu, K.P., & Baldocchi, D.D. (2008). Global estimates of the land–atmosphere water flux based
693 on monthly AVHRR and ISLSCP-II data, validated at 16 FLUXNET sites. *Remote Sensing of*
694 *Environment, 112*, 901-919
695 Fisher, J. B., & ECOSTRESS algorithm development team (2018). ECOsystem Spaceborne Thermal
696 Radiometer Experiment on Space Station (ECOSTRESS): Level-4 Water Use Efficiency L4 (WUE)
697 Algorithm Theoretical Basis Document (ATBD) Rep., 8 pp, Jet Propulsion Laboratory, Pasadena.
698 Franco, A., & Lüttge, U. (2002). Midday depression in savanna trees: coordinated adjustments in
699 photochemical efficiency, photorespiration, CO 2 assimilation and water use efficiency. *Oecologia,*
700 *131*, 356-365

Frankenberg, C., O'Dell, C., Berry, J., Guanter, L., Joiner, J., Köhler, P., Pollock, R., & Taylor, T.E. (2014). Prospects for chlorophyll fluorescence remote sensing from the Orbiting Carbon Observatory-2. *Remote Sensing of Environment, 147*, 1-12

Fredeen, A., & Sage, R. (1999). Temperature and humidity effects on branchlet gas-exchange in white spruce: an explanation for the increase in transpiration with branchlet temperature. *Trees, 14*, 161-168

Gitelson, A.A., Peng, Y., Masek, J.G., Rundquist, D.C., Verma, S., Suyker, A., Baker, J.M., Hatfield, J.L., & Meyers, T. (2012). Remote estimation of crop gross primary production with Landsat data. *Remote Sensing of Environment, 121*, 404-414

Guanter, L., Zhang, Y., Jung, M., Joiner, J., Voigt, M., Berry, J.A., Frankenberg, C., Huete, A.R., Zarco-Tejada, P., & Lee, J.-E. (2014). Global and time-resolved monitoring of crop photosynthesis with chlorophyll fluorescence. *Proceedings of the National Academy of Sciences, 111*, E1327-E1333

Griffith, G.E., Omernik, J.M., Smith, D.W., Cook, T.D., Tallyn, E., Moseley, K., and Johnson, C.B. (2016). Ecoregions of California (poster): U.S. Geological Survey Open-File Report 2016–1021, with map, scale 1:1,100,000, http://dx.doi.org/10.3133/ofr20161021

GOES-R Algorithm Working Group and GOES-R Program office, (2018): NOAA Geostationary Operational Environmental Satellite (GOES-16) Series Advanced Baseline Imager (ABI) Level 2 Land Surface Temperature (LST). [land surface temperature]. NOAA National Centers for Environmental Information. doi:10.7289/V52R3PZ8. [access on 1 August 2020]

Hersbach, H., & Dee, D. (2016). ERA5 reanalysis is in production. *ECMWF newsletter, 147*, 5-6

Hook, S.J., Cawse-Nicholson, K., Barsi, J., Radocinski, R., Hulley, G.C., Johnson, W.R., Rivera, G., & Markham, B. (2019). In-Flight Validation of the ECOSTRESS, Landsats 7 and 8 Thermal Infrared Spectral Channels Using the Lake Tahoe CA/NV and Salton Sea CA Automated Validation Sites. IEEE Transactions on Geoscience and Remote Sensing, 58, 1294-1302

Hulley, G., Shivers, S., Wetherley, E., & Cudd, R. (2019). New ECOSTRESS and MODIS land surface temperature data reveal fine-scale heat vulnerability in cities: A case study for Los Angeles County, California. *Remote Sensing, 11*, 2136

Hulley, G.C., & Hook, S.J. (2010). Generating consistent land surface temperature and emissivity products between ASTER and MODIS data for earth science research. *IEEE Transactions on Geoscience and Remote Sensing, 49*, 1304-1315

Jin, Y., Randerson, J.T., & Goulden, M.L. (2011). Continental-scale net radiation and evapotranspiration estimated using MODIS satellite observations. *Remote Sensing of Environment, 115*, 2302-2319

Köhler, P., Frankenberg, C., Magney, T.S., Guanter, L., Joiner, J., & Landgraf, J. (2018). Global Retrievals of Solar-Induced Chlorophyll Fluorescence With TROPOMI: First Results and Intersensor Comparison to OCO-2. *Geophysical Research Letters, 45*, 10,456-410,463

735 Lawrence, D.M., Fisher, R.A., Koven, C.D., Oelson, K.W., Swenson, S.C. et al. (2019). The Community
736 Land Model version 5: Description of new features, benchmarking, and impact of forcing uncertainty.
737 *Journal of Advances in Modeling Earth Systems*, 11, 4245-4287.
738 Li, K., Guan, K., Jiang, C., Wang, S., Peng, B., Cai, Y. (2020). Validation of land surface temperature
739 products from MODIS, ECOSTRESS, Landsat, GOES-R, VIIRS and Sentinel-3 benchmarked on in
740 situ measurements in the US Corn Belt. *AGU Fall Meeting 2020*. AGU.
741 Li, X., & Xiao, J. (2019a). Mapping photosynthesis solely from solar-induced chlorophyll fluorescence: A
742 global, fine-resolution dataset of gross primary production derived from OCO-2. *Remote Sensing*, 11,
743 2563. https://doi.org/10.3390/rs11212563.
744 Li, X., & Xiao, J. (2019b). A global, 0.05-degree product of solar-induced chlorophyll fluorescence derived
745 from OCO-2, MODIS, and reanalysis data. *Remote Sensing, 11*, 517.
746 https://doi.org/10.3390/rs11050517.
747 Li, X., & Xiao, J. (2020). Global climatic controls on interannual variability of ecosystem productivity:
748 Similarities and differences inferred from solar-induced chlorophyll fluorescence and enhanced
749 vegetation index. *Agricultural and Forest Meteorology*, 108018
750 Li, X., Xiao, J., He, B., Altaf Arain, M., Beringer, J., Desai, A.R., Emmel, C., Hollinger, D.Y., Krasnova,
751 A., & Mammarella, I. (2018). Solar-induced chlorophyll fluorescence is strongly correlated with
752 terrestrial photosynthesis for a wide variety of biomes: First global analysis based on OCO-2 and flux
753 tower observations. *Global Change Biology, 24*, 3990-4008
754 Lin, C., Gentine, P., Frankenberg, C., Zhou, S., Kennedy, D., & Li, X. (2019a). Evaluation and mechanism
755 exploration of the diurnal hysteresis of ecosystem fluxes. *Agricultural and Forest Meteorology, 278*,
756 107642
757 Lin, S., Li, J., Liu, Q., Li, L., Zhao, J., & Yu, W. (2019b). Evaluating the Effectiveness of Using Vegetation
758 Indices Based on Red-Edge Reflectance from Sentinel-2 to Estimate Gross Primary Productivity.
759 *Remote Sensing, 11*, 1303
760 Liu, J., Chen, J., Cihlar, J., & Park, W. (1997). A process-based boreal ecosystem productivity simulator
761 using remote sensing inputs. *Remote Sensing of Environment, 62*, 158-175
762 Liu, L., Guan, L., & Liu, X. (2017). Directly estimating diurnal changes in GPP for C3 and C4 crops using
763 far-red sun-induced chlorophyll fluorescence. *Agricultural and Forest Meteorology, 232*, 1-9
764 Ma, S., Osuna, J.L., Verfaillie, J., & Baldocchi, D.D. (2017). Photosynthetic responses to temperature
765 across leaf–canopy–ecosystem scales: a 15-year study in a Californian oak-grass savanna.
766 *Photosynthesis Research, 132*, 277-291

767 Mäkelä, A., Kolari, P., Karimäki, J., Nikinmaa, E., Perämäki, M., & Hari, P. (2006). Modelling five years
768 of weather-driven variation of GPP in a boreal forest. *Agricultural and Forest Meteorology, 139*, 382-
769 398
770 Nagler, P.L., Cleverly, J., Glenn, E., Lampkin, D., Huete, A., & Wan, Z. (2005). Predicting riparian
771 evapotranspiration from MODIS vegetation indices and meteorological data. *Remote Sensing of*
772 *Environment, 94*, 17-30
773 Omernik, J.M. (1987). Ecoregions of the conterminous United States. *Annals of the Association of*
774 *American geographers, 77*, 118-125
775 ORNL DAAC. 2018. MODIS and VIIRS Land Products Global Subsetting and Visualization Tool. ORNL
776 DAAC, Oak Ridge, Tennessee, USA. Accessed March 24, 2020. Subset obtained for MCD43A4
777 product at various sites in Spatial Range: N=64.87N, S=31.73N, E=70.83W, W=147.86W, time period:
778 2018-01-01 to 2019-12-31, and subset size: 1 x 1 km. https://doi.org/10.3334/ORNLDAAC/1379
779 Otkin, J.A., Anderson, M.C., Hain, C., Mladenova, I.E., Basara, J.B., & Svoboda, M. (2013). Examining
780 rapid onset drought development using the thermal infrared–based evaporative stress index. *Journal*
781 *of hydrometeorology, 14*, 1057-1074
782 Paul-Limoges, E., Damm, A., Hueni, A., Liebisch, F., Eugster, W., Schaepman, M.E., & Buchmann, N.
783 (2018). Effect of environmental conditions on sun-induced fluorescence in a mixed forest and a
784 cropland. *Remote Sensing of Environment, 219*, 310-323
785 Quinlan, J.R. (1992). Learning with continuous classes. In, *5th Australian joint conference on artificial*
786 *intelligence* (pp. 343-348): World Scientific
787 Reichstein, M., Falge, E., Baldocchi, D., Papale, D., Aubinet, M., Berbigier, P., et al. (2005). On the
788 separation of net ecosystem exchange into assimilation and ecosystem respiration: Review and
789 improved algorithm. Global Change Biology, 11, 1424–1439. https://doi.org/10.1111/j.1365-
790 2486.2005.001002.x
791 Robinson, N.P., Allred, B.W., Smith, W.K., Jones, M.O., Moreno, A., Erickson, T.A., Naugle, D.E.,
792 & Running, S.W. (2018). Terrestrial primary production for the conterminous United States derived
793 from Landsat 30 m and MODIS 250 m. *Remote Sensing in Ecology and Conservation, 4*, 264-280
794 Running, S.W., Nemani, R.R., Heinsch, F.A., Zhao, M., Reeves, M., & Hashimoto, H. (2004). A continuous
795 satellite-derived measure of global terrestrial primary production. *AIBS Bulletin, 54*, 547-560
796 Ryu, Y., Baldocchi, D.D., Kobayashi, H., van Ingen, C., Li, J., Black, T.A., Beringer, J., Van Gorsel, E.,
797 Knohl, A., & Law, B.E. (2011). Integration of MODIS land and atmosphere products with a coupled-
798 process model to estimate gross primary productivity and evapotranspiration from 1 km to global
799 scales. *Global Biogeochemical Cycles, 25*

Ryu, Y., Baldocchi, D.D., Black, T.A., Detto, M., Law, B.E., Leuning, R., Miyata, A., Reichstein, M., Vargas, R., & Ammann, C. (2012). On the temporal upscaling of evapotranspiration from instantaneous remote sensing measurements to 8-day mean daily-sums. *Agricultural and Forest Meteorology, 152*, 212-222

Schubert, P., Eklundh, L., Lund, M., & Nilsson, M. (2010). Estimating northern peatland CO2 exchange from MODIS time series data. *Remote Sensing of Environment, 114*, 1178-1189

Silvestri, M., Romaniello, V., Hook, S., Musacchio, M., Teggi, S., Buongiorno, M. (2020). First Comparisons of Surface Temperature Estimations between ECOSTRESS, ASTER and Landsat 8 over Italian Volcanic and Geothermal Areas. *Remote Sensing*, 12(1): 184.

Sims, D.A., Rahman, A.F., Cordova, V.D., Baldocchi, D.D., Flanagan, L.B., Goldstein, A.H., Hollinger, D.Y., Misson, L., Monson, R.K., & Schmid, H.P. (2005). Midday values of gross CO2 flux and light use efficiency during satellite overpasses can be used to directly estimate eight-day mean flux. *Agricultural and Forest Meteorology, 131*, 1-12

Sims, D.A., Rahman, A.F., Cordova, V.D., El-Masri, B.Z., Baldocchi, D.D., Bolstad, P.V., Flanagan, L.B., Goldstein, A.H., Hollinger, D.Y., & Misson, L. (2008). A new model of gross primary productivity for North American ecosystems based solely on the enhanced vegetation index and land surface temperature from MODIS. *Remote Sensing of Environment, 112*, 1633-1646

Stocker, B.D., Wang, H., Smith, N.G., Harrison, S.P., Keenan, T.F., Sandoval, D., Davis, T., & Prentice, I.C. (2020). P-model v1. 0: an optimality-based light use efficiency model for simulating ecosystem gross primary production. Geoscientific Model Development, 13, 1545-1581

Su, Z. (2002). The Surface Energy Balance System (SEBS) for estimation of turbulent heat fluxes. *Hydrology and Earth System Sciences, 6*, 85-99

Turner, A.J., Köhler, P., Magney, T.S., Frankenberg, C., Fung, I., & Cohen, R.C. (2020). A double peak in the seasonality of California's photosynthesis as observed from space. Biogeosciences, 17, 405-422

Wagle, P., & Kakani, V.G. (2014). Environmental control of daytime net ecosystem exchange of carbon dioxide in switchgrass. *Agriculture, Ecosystems & Environment, 186*, 170-177

Wang, C., Guan, K., Peng, B., Chen, M., Jiang, C., Zeng, Y., Wu, G., Wang, S., Wu, J., & Yang, X. (2020). Satellite footprint data from OCO-2 and TROPOMI reveal significant spatio-temporal and inter-vegetation type variabilities of solar-induced fluorescence yield in the US Midwest. *Remote Sensing of Environment, 241*, 111728

Wolanin, A., Camps-Valls, G., Gómez-Chova, L., Mateo-García, G., van der Tol, C., Zhang, Y., & Guanter, L. (2019). Estimating crop primary productivity with Sentinel-2 and Landsat 8 using machine learning methods trained with radiative transfer simulations. *Remote Sensing of Environment, 225*, 441-457

Wutzler, T., Lucas-Moffat, A., Migliavacca, M., Knauer, J., Sickel, K., Šigut, L., Menzer, O., & Reichstein, M. (2018). Basic and extensible post-processing of eddy covariance flux data with REddyProc. *Biogeosciences, 15,* 5015-5030

Xia, J., Niu, S., Ciais, P., Janssens, I.A., Chen, J., Ammann, C., Arain, A., Blanken, P.D., Cescatti, A., & Bonal, D. (2015). Joint control of terrestrial gross primary productivity by plant phenology and physiology. *Proceedings of the National Academy of Sciences, 112*, 2788-2793

Xiao, J., Chevallier, F., Gomez, C., Guanter, L., Hicke, J.A., Huete, A.R., Ichii, K., Ni, W., Pang, Y., Rahman, A.F., Sun, G., Yuan, W., Zhang, L., Zhang, X. (2019) Remote sensing of the terrestrial carbon cycle: A review of advances over 50 years. *Remote Sensing of Environment*, 233, 111383. https://doi.org/10.1016/j.rse.2019.111383.

Xiao, J., Ollinger, S.V., Frolking, S., Hurtt, G.C., Hollinger, D.Y., Davis, K.J., Pan, Y., Zhang, X., Deng, F., & Chen, J. (2014). Data-driven diagnostics of terrestrial carbon dynamics over North America. *Agricultural and Forest Meteorology, 197*, 142-157

Xiao, J., Zhuang, Q., Baldocchi, D.D., Law, B.E., Richardson, A.D., Chen, J., Oren, R., Starr, G., Noormets, A., & Ma, S. (2008). Estimation of net ecosystem carbon exchange for the conterminous United States by combining MODIS and AmeriFlux data. *Agricultural and Forest Meteorology, 148*, 1827-1847

Xiao, J., Zhuang, Q., Law, B.E., Baldocchi, D.D., Chen, J., Richardson, A.D., Melillo, J.M., Davis, K.J., Hollinger, D.Y., & Wharton, S. (2011). Assessing net ecosystem carbon exchange of US terrestrial ecosystems by integrating eddy covariance flux measurements and satellite observations. *Agricultural and Forest Meteorology, 151*, 60-69

Xiao, J., Zhuang, Q., Law, B.E., Chen, J., Baldocchi, D.D., Cook, D.R., Oren, R., Richardson, A.D., Wharton, S., & Ma, S. (2010). A continuous measure of gross primary production for the conterminous United States derived from MODIS and AmeriFlux data. *Remote Sensing of Environment, 114*, 576-591

Xu, H., Xiao, J., & Zhang, Z. (2020). Heatwave effects on gross primary production of northern mid-latitude ecosystems. *Environmental Research Letters, 15*, 074027

Xu, L., & Baldocchi, D.D. (2004). Seasonal variation in carbon dioxide exchange over a Mediterranean annual grassland in California. *Agricultural and Forest Meteorology, 123*, 79-96

Yang, L., Jin, S., Danielson, P., Homer, C., Gass, L., Bender, S.M., Case, A., Costello, C., Dewitz, J., & Fry, J. (2018). A new generation of the United States National Land Cover Database: Requirements, research priorities, design, and implementation strategies. *ISPRS journal of photogrammetry and remote sensing, 146*, 108-123

865 Yu, Y., Tarpley, D., Privette, J.L., Goldberg, M.D., Raja, M.R.V., Vinnikov, K.Y., & Xu, H. (2008).
866 Developing algorithm for operational GOES-R land surface temperature product. *IEEE Transactions*
867 *on Geoscience and Remote Sensing, 47*, 936-951
868 Zhao, M., Heinsch, F.A., Nemani, R.R., & Running, S.W. (2005). Improvements of the MODIS terrestrial
869 gross and net primary production global data set. *Remote Sensing of Environment, 95*, 164-176
870
871